Review



# Lab-on-Chip for Cell Sorting: Main Features and Advantages of Inertial Focusing in Spiral Microchannels

Isabella Petruzzellis , Rebeca Martínez Vázquez * , Stefania Caragnano , Caterina Gaudiuso , Roberto Osellame * , Antonio Ancona , Annalisa Volpe *

Posted Date: 19 July 2024

doi: 10.20944/preprints202407.1511.v1

Keywords: Cell sorting; Inertial Microfluidics; Particle manipulation; Lab-on-Chip

*Review*

# Lab-on-Chip for Cell Sorting: Main Features and Advantages of Inertial Focusing in Spiral Microchannels

**Isabella Petruzzellis [1], R. Martínez Vázquez [2,*], Stefania Caragnano [1], Caterina Gaudiuso [3], Roberto Osellame [2], Antonio Ancona [1,3] and Annalisa Volpe [1,3,*]**

[1] Physics Department, Università degli Studi di Bari & Politecnico di Bari, Via Orabona 4, 7016 Bari, Italy; isabellapetruzzellis97@gmail.com (I.P), stefania.caragnano@poliba.it (S.C.), antonio.ancona@uniba.it (A.A.); annalisa.volpe@poliba.it (A.V.)

[2] Institute for Photonics and Nanotechnologies (IFN), CNR, Piazza L. da Vinci 32, 20133 Milan, Italy; rebeca.martinezvazquez@cnr.it (R.M.V); roberto.osellame@cnr.it (R.O.)

[3] Institute for Photonics and Nanotechnologies (IFN), CNR, Via Amendola 173, 70125 Bari, Italy; caterina.gaudiuso@cnr.it (C.G.)

* Correspondence: rebeca.martinezvazquez@cnr.it (R.M.V.); annalisa.volpe@poliba.it (A.V.)

**Abstract:** Inertial focusing based Lab-on-Chips represent nowadays a promising technology for cell sorting in various applications, thanks to their coherence with the *ASSURED* criteria recommended by the World Health Organization, being: Affordable, Sensitive, Specific, User-friendly, Rapid and Robust, Equipment-free and Delivered. Inertial focusing in spiral microchannel can offer a rapid, portable and ease of prototyping solution for cell-sorting. In literature, different geometries of microfluidic channel have been investigated to understand how hydrodynamic forces, due to primary and secondary flow, influence particle focusing. The balancing of these forces in spiral microchannels allows for high throughput and filtration efficiency across different particle and sizes. The understanding of such mechanism represents a key aspect to address the prototyping of spiral devices for the target application. A clear, complete and orderly overview in the current literature is lacking. For this reason, we aim to compare the main features of inertial focusing depending on various cross-section (rectangular, trapezoidal, triangular, hybrid) in spiral devices. Additionally, details about materials and prototyping techniques will be provided. This review study will provide readers a comprehensive overview of current research, guiding future experimentation by expediting the selection of spiral geometries and materials based on the type of particle to be separated.

**Keywords:** cell sorting; inertial microfluidics; particle manipulation; lab-on-chip

## 1. Introduction

Since the latter half of the last century, the scientific community has recognized the need to optimize existing chemical, biological, and clinical analysis techniques.

Cell sorting in one of the primary purposes in cells analysis and involves the analysis of cell samples and differentiation into their respective subcellular components within a heterogeneous mixture. The applications of this technique embrace from the study of bacteria and pathogens in the food and environmental sectors [1,2], the cultivation of stem cells for tissue and organ regeneration [3,4], the separation of tumor cells from blood sample for early cancer diagnosis [5–8]. For example, the possibility of isolating stem cells from bone tissue with high purity can improve proliferative and regeneration capacity; also isolating Circulating Tumor Cells (CTCs) from Blood Cells (BCs) enables cancer diagnosis in initial stages [9] considering CTCs isolation a real-time "liquid biopsy". However,

 doi:10.20944/preprints202407.1511.v1



CTCs are extremely rare in a blood sample, making their isolation and characterization an extreme technological challenge [10].

It is important to consider all practical aspects involved when choosing a sorting technique. First, ease of execution, reduced instrumental dimensions and energies, high separations speed and minimized biological risk for the operator could improve the operational logistic and the time required. Then, versatility, accuracy, sensitivity, ability to analyze small amount of biological fluids consisting of a large variety of cells make the technique chosen suitable for different applications and biological matrixes [11].

The need to integrate the earlier-mentioned properties into a single separation technique has led researchers to study and design different cells sorting systems; for example, miniaturized devices, based on microfluidic principles, can address this aim. Compared to conventional sorting techniques, like fluorescence-activated cell sorting (FACS) [12], magnetically activated cell sorting (MACS) [13], and centrifugation methods [14], which faced some technical limits, recent microfluidic techniques applied to cells extraction offer numerous advantages. While conventional sorting techniques require labeled cells, long processing times, high operating costs and energies and bulky equipment despite they offer high efficiency [11], recent microfluidic techniques allow label-free cell sorting, reduced time and power operation, sample volumes and lower equipment fabrication costs thanks to the use of miniaturized devices. Label-free cell sorting techniques rely on cell characteristics such as physicochemical, immunological, and functional properties (size, volume, density, refraction index, membrane potential, pH, electrical impedance, and charge) [15].

These techniques can be categorized into i) active separation and ii) passive separation. Active separation technologies involve external forces, such as electric or electromagnetic fields, requiring high space, expensive or bulky external generators often offering a low throughput. These include dielectrophoresis (DEP) [16], magnetophoresis (MAP) [17], acoustophoresis [18], and optical tweezers [19]. Passive separation techniques, in contrast, do not require external forces allowing cell sorting depending on microchannel geometry and intrinsic hydrodynamic characteristics, offering a higher throughput than active techniques. Cell throughput is defined as the number of cells that can be handled within the time it takes to perform the sorting. For active techniques the external force takes a long amount of time to overcome the hydrodynamic drag acting on the particles. This problem has been solved in passive techniques thanks to the only action of fluid inertia [20,21].

One of passive techniques advantage is the possibility to integrate the microfluidic sorting system in miniaturized devices, known as Lab-on-Chips (LoCs). The growth of LoC since 1970s, driven by the development of Micro-Electro-Mechanical-System (MEMS), has addressed these requirements. LoCs are miniaturized microfluidic devices, typically a few square centimeters in size, capable of manipulating small volumes of fluids through the implementation of micrometer-sized channels, pumps, and tubes allowing rapid diagnostics and therapy. George Whitesides, a pioneer of microfluidics, defined it as “the science and technology of systems that manipulate small quantities of fluids through channels 10 to 100 micrometers in size” [22].

Therefore, microfluidic devices represent a promising technology for point-of-care testing ad diagnosis and adhere to the criteria recommended by the World Health Organization (WHO) to be Affordable, Sensitive, Specific, User-friendly, Rapid and Robust, Equipment-free and Delivered to those who need it, i.e., ASSURED [23].

Among passive techniques, the main ones are pinched flow fractionation (PFF) [24], deterministic lateral displacement (DLD) [25], hydrophoretic filtration [26], size exclusion filtration [27], crossflow filtration [28], and inertial focusing [29,30].

Pinched flow fractionation (PFF) involves injecting the flow containing cells, first, into a narrow channel and then into a wider chamber, forcing cells to align at a distance from the channel wall depending on their size: smaller cells align closer to the wall than larger cells [24]. On the other hand, deterministic lateral displacement (DLD) involves placing a periodic array of micro-obstacles in the channel of the device, directing smaller particles in one direction and larger particles in another direction defined by the positioning of the obstacles [25]. Hydrophoretic filtration, similar to DLD, utilizes a periodic array of step-like obstacles inside the channel, creating a pressure gradient that

 doi:10.20944/preprints202407.1511.v1



directs particles of lower density to different zones than particles of higher density [26]. In the size exclusion filtration method, a columnar micro-obstacle pattern allows for the selection of cell groups based on their size and shape [27]. Cross-flow filtration technique, instead, relies on a membrane with pores that retain particles of larger size [30].

Inertial focusing techniques exploit the action of inertial forces acting on particles suspended in a fluid within a microchannel. They are based on inertial effects which arise between the Stokes linear regime and turbulent fluid regime [31] Inertial and viscous forces act on particles in a fluid confined in a micrometer channel, making them to migrate towards some equilibrium positions. Channel and particles dimensions and geometry play a role in this effect, resulting in lateral migration in straight channels [30,32] and Dean secondary flows in channels with a curvature (i.e., serpentine, spiral channels) [33,34]. Additionally, the microchannel cross-sectional shape could influence how inertial and viscous forces balance themselves, and consequently, affect particle behavior.

Inertial particle sorting using spiral microchannels with different cross-sections requires further numerical simulations and experimental studies in order to understand how different experimental conditions, such as channel dimensions, cells type, channel cross-sectional shape affect particle behavior. Therefore, a well-organized and clear review of the existing literature is essential to guide future research in this field.

This review aims to provide a comprehensive overview of the developments and advantages of inertial focusing in spiral microchannels used as cell sorting technique, starting with a description of the physical phenomenon. We begin by discussing the inertial sorting mechanism in straight micrometric channels, followed by an exploration of how curvature in channel geometry enhances particle migration to achieve better equilibrium positions. Subsequently, common materials and methods used for spiral inertial-based Lab-on-Chip (LoC) fabrication and testing will be presented. An in-depth survey of geometries investigated in the literature is conducted, with a specific focus on the influence of channels' cross-sectional shape on the sorting efficiencies based on the sizes of the particles to be separated. Various successful outcomes have been achieved in sorting different types of particles (CTCs, bacteria, viruses, blood cells) by modifying the cross-sectional geometry.

## 2. Theoretical Backgrounds: Inertial Focusing

Lateral migration was first studied in 1960 by Segrè and Silberberg [35]. Their experiment consisted in the observation of neutrally buoyant microscopic polymethylmethacrylate spherical particles flowing in a viscous fluid; a neutrally buoyant particle neither sinks nor floats when placed in a fluid, whose density matches the density of the particle. As a result, the gravitational force is balanced by the buoyant force pushing the particle up, leading to a state where the particle remains suspended at a constant depth or position within the fluid.

Then, they observed that the spheres, flowing in a viscous fluid in a straight tube with a circular section and hydraulic diameter $D_h = 1$ cm, positioned in a circular arrangement within the tube section at a distance of $0.2 \cdot D_h$ from the walls Figure 1; the hydraulic diameter is defined as [36]:

$$D_h = \frac{4\ x\ cross\ sectional\ area}{cross\ sectional\ perimeter} \quad (1)$$

which, for a circular channel, is equal to the diameter of the circular cross-section.

This effect was named the "Tubular pinch effect". They also asserted that this effect could find applications in the fractionation of particles of different sizes [35].

 doi:10.20944/preprints202407.1511.v1



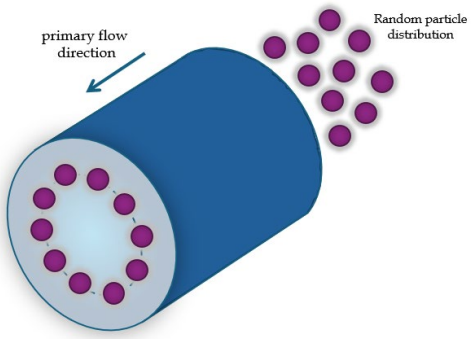


**Figure 1.** schematic representation of the "Tubular pinch effect".

This effect has been studied a lot through years, in order to understand the behavior of particles flowing in a tube [32]. Particle behaviour in the fluid depends on the flow regime which is defined by the Reynolds number $R_e$, a dimensionless number defined as the ratio between inertial forces and viscous forces calculated as:

$$R_e = \rho U_f D_h / \mu \quad (2)$$

with $\rho$ the fluid density, $U_f$, the average velocity of the fluid and $\mu$ the dynamic viscosity. As expected, in microfluidic devices $R_e$ is extremely low (between $10^{-6}$ and 10) resulting in that inertial effects can be ignored. However, in microchannels where a laminar flow regime with $R_e < 2000$ is established, inertial effects appear ([36,37]).

In rectilinear microfluidic tubes, for moderate $R_e$ $(1 < R_e < 10^2)$, inertial forces dominate over viscous forces; in this $R_e$ conditions the flow is laminar and not turbulent and is called Poiseuille flow. When a fluid is confined by channel walls, the velocity profile of the fluid is parabolic as the friction of the walls tends to slow the fluid's streamlines. The fluid velocity gradient induces the particle to be retarded in perpendicular and parallel directions respect to the walls due to drag caused by walls, resulting in the emergence of Magnus lift-force, Saffman force and wall-lift force [10,31,38].

Magnus lift-force is a consequence of particle rotation due to the fluid velocity gradient around the particle and acts perpendicular to both the rotation axis and the particle motion [31]. The rotation induces fluid circulation around the particle: the fluid velocity on the upper part of the particle increases, streamlines are closer, and the pressure is low, while the fluid velocity on the lower part of the particle decreases, the streamlines are more spaced, and the pressure is higher. Then, as a result of the transverse pressure gradient, caused by the asymmetry in the flow streamline, a lift is generated [36].

The drag caused by walls exerts a lateral force on the particle known as the Saffmann force. It arises from the interaction between the particle's velocity field and the flow velocity gradient and acts towards the channel wall. The Saffman force is defined as:

$$F_s = \frac{K}{4} V a^2 (\gamma v^{-1})^{\frac{1}{2}} \quad (3)$$

where $K$ is a constant, $V$ is the relative velocity between the particles and the fluid, $a$ the particle diameter, $\gamma$ is the velocity gradient, and $v$ the kinetic viscosity. When the particles are neutrally buoyant in a Poiseuille flow, no Saffman force acts on the particles.

As, said before, the presence of the walls modifies the flow field around the particle, causing the particle motion to be retarded in the parallel and perpendicular directions with respect to the primary flow [10]. A lateral migration of the particle emerges as the consequence of two forces perpendicular to the primary fluid flow: i) the $F_{LS}$ shear-lift force, and ii) the $F_{LW}$ wall-lift force (Figure 2).

Preprints.org (www.preprints.org) | NOT PEER-REVIEWED | Posted: 19 July 2024 doi:10.20944/preprints202407.1511.v1



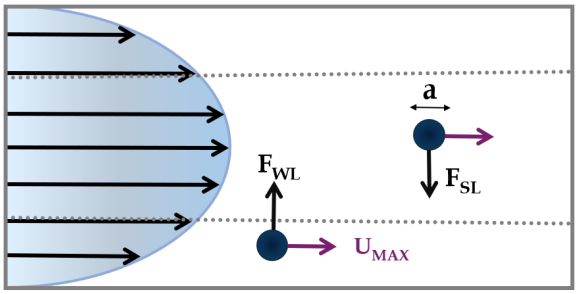


**Figure 2.** Balancing of wall-lift force and shear-lift force acting on particle in a rectilinear channel.

The first acts radially from the center towards the channel walls and derives from the parabolic velocity profile of the liquid; it is defined as:

$$F_{LS} = \frac{f_{LS}\,\rho\,U_{max}^2\,a^3}{D_h} \quad (4)$$

where $f_{LS}$ is the shear-lift coefficient, ρ is the particle density, $U_{max}$ is the maximum velocity, a is the particle diameter; $D_h$ is the channel hydraulic diameter, equal to the diameter of the circular cross-section for a circular channel or defined as $D_h = 2wh\,/(w+h)$ for a rectangular channel (where $w$ is the width and $h$ the height of the cross-section).

The second force arises from the interaction between particles and the tube walls. It is directed towards the tube center [39] and is defined as:

$$F_{LW} = \frac{f_{LW}\,\rho\,U_{max}^2\,a^6}{D_h} \quad (5)$$

where $f_{LW}$ is the wall-lift coefficient.

The balance between $F_{LS}$ and $F_{LW}$ defines the net inertial force, derived by Asmolov [40]:

$$F_L = f_L\,\frac{\rho\,U_{max}^2\,a^4}{D_h} \quad (6)$$

where $f_L$ is the lift coefficient, which is a function of the lateral particle position and $R_e$ ($f_L \propto \frac{H^2}{a^2}\sqrt{Re}$). Under this force, a small spherical particle with $\frac{a}{D_h} \ll 1$ [40] migrates towards distinct equilibrium positions, across the streamlines. The net inertial force acting on the particles then, has a biquadratic dependence on particle size ($F_L \propto a^4$) and on geometric properties of the channel.

The particles' Reynolds number $R_p$, which is defined as:

$$R_p = R_e\left(\frac{a}{D_h}\right)^2 = \frac{\rho U_f}{\mu\,D_h}. \quad (7)$$

and takes into account the size ratio of the particle to the channel and can predict particle fluid dynamic behaviour. For $R_p$ on the order of 1, the inertial lift force becomes dominant, leading particles to migrate towards distinct equilibrium positions; conversely, when $R_p \ll 1$, particles are subject to the dominant viscous drag, following fluid streamlines [41].

First, in 2007 Di Carlo et al. [33], predicted theoretically and demonstrated trough experiments with particles of different sizes, that for the particles to reach the equilibrium position it is necessary that $a/D_h > 0.07$. The same result was experimentally demonstrated by [42].

As seen, the hydraulic diameter influences the particle behavior and, consequently, the width and the height of the channel. Another important criterion is the aspect ratio $AR$ of the microfluidic channel, defined as the ratio between its width and height.

In circular cross-section channels, particles migrate forming an annulus [35,43]. In square section channels with an aspect ratio AR of 1, four equilibrium positions are observed at the center of each channel walls [33]. In rectangular section channels with an aspect ratio AR greater or less than 1, there is a reduction of equilibrium positions from four to two, located in the midpoint of each channel longer walls [30].

In solutions with particles of various sizes, flowing in rectilinear channels a low value of the ratio ($AR \approx 0.5$), makes larger particle reach their focusing equilibrium positions faster, while smaller ones reach their equilibrium position after flowing a sufficiently long distance. The minimum required length $L_{MIN}$ to achieve focusing can be estimated by [44]:

 doi:10.20944/preprints202407.1511.v1



$$L_{MIN} = \frac{3\pi\,\mu\,D_h^3}{\rho\,U\,a^3}. \quad (8)$$

having a cubic dependence on $1/(\frac{a^3}{L_c^3})$, where $L_c$ is the characteristic length the microchannel; for square cross-sectional microchannels, $L_c$ is equal to the microchannel hydraulic diameter $D_h$, while for rectangular cross-sectional microchannels is equal the narrowest channel dimension by [44].

Despite the operational and fabrication ease of straight channels, to allow particle to reach the necessary $L_{MIN}$ for focusing on equilibrium positions, microchannels have to be designed with a high side length which implies higher flow resistance and a large device footprint.

The inefficiency in separating cells with different sizes in straight microchannels has led to the design of curvilinear microchannels with a low aspect ratio ($AR < 1$) [10]. Curvilinear microchannels include serpentine or spiral geometries; while serpentine channels have alternating curvature, spiral channel has a curvature along a single direction.

### *2.1. Curvilinear Microchannel and Dean Vortices*

Introducing a curvature with a radius $R_c$ in the channel geometry, a secondary flow or Dean flow arises due to the flow velocity difference in the downstream direction between fluid in the central and in the near-walls region of the channel [45]. Fluid elements around the tube center move in circular motions, creating a radial pressure gradient directed towards the upper and lower tube walls. This leads to the formation of two symmetrical vortices perpendicular to the main flow direction (Figure 3a).

The distribution and strength of these vortices are related to a dimensionless parameter, the Dean's number:

$$De = R_e\sqrt{\frac{D_h}{2\,r_c}} \quad (9)$$

with $R_e$ Reynolds number, $D_h$ diameter of the hydraulic channel and $r_c$ radius of curvature of the convex surface of the curvilinear channel.

Hence, particles in a curvilinear channel experience both the net inertial force $F_L$ and the drug force:

$$F_{Dean} = 3\pi\,\mu\,a\,U_D \quad (10)$$

where $U_D = 1.8\cdot 10^{-4}\,De^{1.63}$ is the Dean velocity, i.e., the lateral migration velocity of the particles [46].

The competition between the net inertial force $F_L$ and the drug force $F_{Dean}$ determines migration towards the equilibrium positions in a curvilinear microchannel. It must be underlined that the Dean force does not contribute to creating focusing positions, but it acts additionally to inertial forces to reduce the number of equilibrium positions; consequently, particles migrating to different locations become unstable and return to initial equilibrium positions [33].

Along a Dean vortex, a particle undergone a lateral distance traversed defined as "Dean cycle; under a Dean cycle a particle migrates from a channel wall to the opposite wall and then returns to the initial position as presented in the simulation in Figure 3b. The length for one Dean cycle migration can be calculated as $L_{DC} \approx 2w + h$ where $w$ is the microchannel width and $h$ is the microchannel height [47]. So, the total microchannel length required for the particle to reach Dean migration is given by $L_C = \frac{U_F}{U_D} L_{DC}$ . In the ideal condition, Dean drag force is of the same order as the net inertial lift leading particles to reach the lift-induced equilibrium positions interacting weakly with the Dean flow. If $F_L$ is greater than $F_{Dean}$, then the focusing mechanism is continually interrupted and if $F_L$ is weaker than $F_{Dean}$ then the focusing will be only due to inertial lift. As suggested by [33] the ratio of lift to drug force scales as:

$$\frac{F_L}{F_{Dean}} \sim \left(\frac{D_h}{2r_c}\right)^{-1}\left(\frac{a}{D_h}\right)^3 R_e \quad (11)$$

from which it can be noted that as $D_h/2r_c$ and $De$ approaches 0 (i.e., straight channels), the Dean drug force dominates on the net inertial force and the particles remain confined within the Dean vortices. The third-power dependence on the ratio of particle to channel dimensions suggests that a smaller particle could be not focused, whereas a larger particle focuses quickly. Conversely, as

Preprints.org (www.preprints.org) | NOT PEER-REVIEWED | Posted: 19 July 2024 doi:10.20944/preprints202407.1511.v1



$D_h/2r_c$, and $De$ approache to ∞ the net inertial force dominates over the Dean force and the mechanism is likewise that observed in straight channels with all particles that will be defocused.

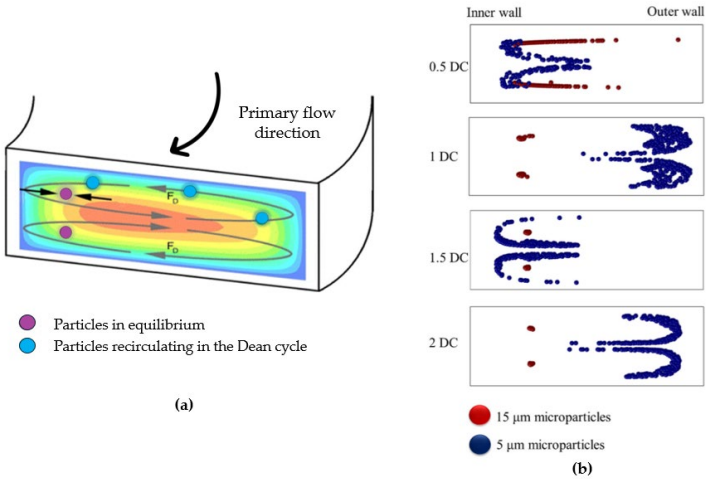


**Figure 3.** (a) Schematic representation of secondary flow and Dean vortices; (b) Simulation of cross-sectional position of a 5 and 15 µm microparticles mixture in a spiral microchannel, showing Dean cycles [7].

Therefore, the hydraulic diameter dependence implies that particles undergo weaker inertial forces and stronger Dean drag force as channel dimensions increase [48].

The dependence of the Dean number on the radius of curvature $r_c$ draws attention to the type of spiral chosen. One of the most studied in this regard is the Archimedes spiral; this can be defined as a curve where each loop is spaced from the next one by a constant amount. The constant increase of the radius of curvature has been shown to induce a gradual development of vortices due to the secondary flow, thus affecting the minimum focusing length [34].

### *2.2. Rectangular and Trapezoidal Spiral Microchannels*

As explained in section 2, the cross-section geometrical properties of the channel play a role in the migration of particles towards equilibrium positions in spiral microchannels.

Different studies have been conducted to understand the focusing mechanisms on spiral channels with square [49], rectangular [50], trapezoidal [51], hybrid cross-sectional shape [52]. In a square channel, particles migrate to four equilibrium positions located near a corner or at the center of an edge of the tube (Figure 4a) [49].

In a rectangular section channel, the interplay between inertial lift force and Dean drag force leads to the formation of symmetrical Dean vortices in the upper and lower sections of the channel. This causes particles to migrate across the channel width until they reach their equilibrium position near the inner or outer wall. In case of a mixture of particles of different sizes, smaller particles will focus towards the center of the channel, while bigger particle will focus nearby the outer wall (Figure 4b).

In a trapezoidal section channel, the symmetry breaking in the channel geometry affects the formation of Dean vortices, as demonstrated by Guan et al. [50]. By varying the inner and the outer wall heights, two asymmetric Dean vortices appear, directing quickly smaller particles towards the outer half of the channel wall and the bigger ones towards the inner half wall, thus providing a clearer difference in equilibrium position [53]. Due to the stronger vortices, the spacing between the two cell streams is maximized allowing an higher resolution sorting. (Figure 4c). The use of trapezoidal-section spiral channels was first studied by Wu's researchers' group [54]. Since the publication of this work, various studies demonstrated the separation of different types of particles, including the isolation of leukocytes from circulating tumour cells (CTCs) within a blood sample [51], the selective

 doi:10.20944/preprints202407.1511.v1



separation of microalgae cells [55] and the identification of the bacteria responsible for the deterioration of beer [1]. Then, designing hybrid cross section channels, for example combing a trapezoidal and a rectangular geometry, can enhance the focusing mechanism [56].

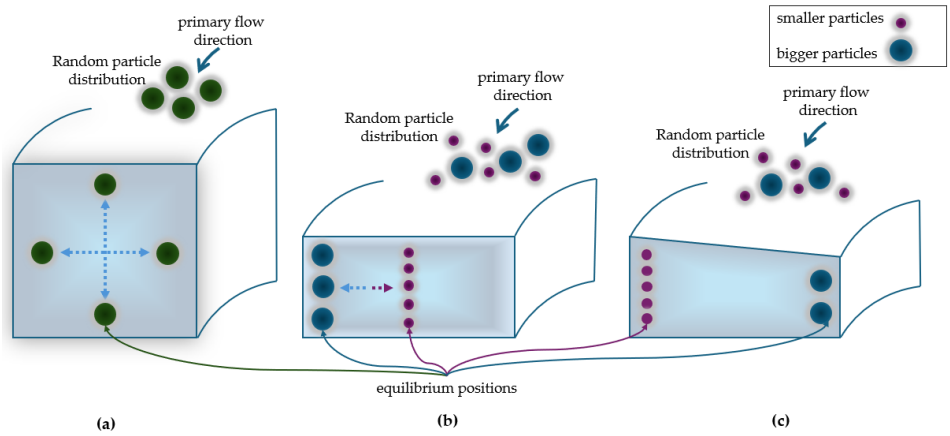


**Figure 4.** Equilibrium positions of particles in (a) squared, (b) rectangular and (c) trapezoidal cross-section channel.

## 3. Materials and Prototyping Techniques for Spiral Microchannels

As seen, Archimedean spiral microfluidics represent an interesting design for prototyping of miniaturized LoCs for cell sorting, thanks to the increases channel length that allows particles focusing on their equilibrium positions. The fabrication process of such channel with different cross-sectional geometries (squared, rectangular, trapezoidal or complex) have to match with the replication process rapidity and ease to be industrially scalable.

Then, the choice of the appropriate prototyping technique for the fabrication of LoCs in addition to the choice of material, must be considered. Many studies have been published about general microfabrication techniques and materials for microfluidics, for example [57–61] works.

In the following paragraph, we will present the most commonly used materials to produce LoCs, highlighting their limitations and advantages for the fabrication of spiral inertial microfluidic chips. Moreover, techniques for rectangular, trapezoidal and complex cross section spiral microchannel will be outlined. A review of the most suitable fabrication techniques is essential since the fabrication of slanted or complex spiral channels can be very expensive due to the difficulty of producing these channels using conventional micromachining methods [62]. All the details regarding the papers discussed in these sections will be summarized in Table 1 to provide the reader with a quick overview.

### *3.1. Materials*

The main used materials for LoCs fabrication can be divided into four categories: i) inorganic materials (i.e., metals, ceramics, and glasses) and ii) organic materials (polymers and biodegradable materials).

Metals, such as iron, aluminium, copper, and their alloys, exhibit desirable properties such as cost-effectiveness, high availability, ease of processing, and good resistance to high temperatures and pressures. However, they may pose challenges in interacting with biological fluids. Noble metals, such as gold or platinum, could enhance biocompatibility, but disadvantages such as high costs or the lack of optical transparency make them not ideal for these applications [57]. For this reason, no metallic spiral microfluidic devices for biological liquids and cells manipulation have been reported.

Apart from metals, commonly used inorganic materials for LoC production include glass, silicon, and ceramics. Silicon has been widely used in recent decades for its availability, chemical compatibility, thermal stability, and possibility to fabricate devices with nanometer resolution.

 doi:10.20944/preprints202407.1511.v1



However, its opacity to visible and UV radiation makes it unsuitable for direct real-time imaging, which is required for cell sorting monitoring and for fluorescent optical detection. Moreover, its poor mechanical properties, such as fragility and high elastic modulus can cause issues when exposed to high-pressure flows. The high costs of fabrication make silicon an inappropriate candidate for low-cost portable Lab-on-Chips. Additionally, due to its lack of gas permeability it cannot be used for long-term cell culture. For these reasons, silicon has been rarely used for microfluidics; the only study of a silicon spiral device fabrication for cell sorting was conducted by Gregoratto et al. [63].

Similarly, glass, being chemically inert and biologically compatible and showing properties like thermal stability and insulation, can be a valuable option in various operational conditions. Compared to silicon, glass, offers advantages such as optical transparency and lower costs but the prototyping of microfluidic structures on glass requires techniques which are time consuming, not suitable for low-cost mass-scale devices fabrication. Ceramics, despite the good corrosion resistance and thermal stability, pose challenges due to their fragility and high porosity. As silicon, due to opacity to visible radiation, real-time imaging is an issue in ceramics-based microfluidic devices.

Inorganic materials are characterized by a scarce gas permeability, which is a major issue that makes them unsuitable as the materials of choice for the fabrication of Lab on Chips for long-term cells manipulation, as required for the inertial sorting of cells and viable organism, such as bacteria, algae and yeast [59].

Polymeric materials have been widely used for microfluidic devices fabrication, especially on a large industrial scale, due to the ease and cost-effectiveness of processing. Moreover, thanks to biocompatibility and optical transparency or semi-transparency in the visible range, polymers are the best candidates for cell sorting applications. Polymers are categorized as thermosetting and thermoplastic [64]. The most used polymers include polydimethylsiloxane (PDMS), fluoropolymers (TEFLON, PTFE), and polymethylmethacrylate (PMMA). PDMS, a thermosetting polymer, is used in most microfluidic devices thanks to its hydrophobicity, gas permeability, optical transparency, biocompatibility, and high elasticity. Disadvantages of using PDMS are that it may exhibit issues such as channel deformation due its high mechanical compliance, evaporation and adsorption, leaching-out of uncrosslinked oligomers, and hydrophobic recovery over time, after hydrophilic treatment [60]. Despite these aspects, PDMS is the most widely used polymer for spiral microchannel fabrication for cell sorting in association with the soft-lithography technique that will be explained later.

PMMA, a thermoplastic polymer, has been used due to its low production costs and its ability to be reused after decomposition at temperatures above the glass transition temperature ($T_g$), making it ideal for sustainable “green microchips” fabrication [65]. It exhibits high rigidity, which is optimal for applications requiring high pressures, optical transparency in the visible range, excellent mechanical and electrical properties, solvent compatibility except for organic solvents and hydrocarbons. Even if it is still less used than PDMS, PMMA represents an optimal candidate for rigid spiral microchannel devices allowing the application of high operating flow rates without leakage [2,66]

Last category is biodegradable materials, such as paper, hydrogels and wax. Paper has become an interesting material for chip fabrication due to its numerous properties such as low costs, bio-affinity, accessibility, lightweight, and ease of fabrication; however, it lacks mechanical resistance in the presence of liquids and transparency. Hydrogels, are three-dimensional structures of hydrophilic polymer chains and allow diffusion of bioparticles and small molecules, presenting high biocompatibility, biodegradability, and low toxicity. However, the difficulty in maintaining device integrity and channel geometry in hydrogels under different operational conditions, such as high-pressure flows required in inertial focusing in micrometer channels, make them challenging to use [67–69].

### *3.2. Fabrication Techniques*

In a study published in 2011, Waldbaur et al. [70] categorized the fabrication techniques of microfluidic devices into two main categories based on whether the microchannels structure is

 doi:10.20944/preprints202407.1511.v1



replicated or not: i) by deposition of material (replication techniques via mold) or ii) by direct material removal. In the text that follows, we have chosen to use this categorization to review the techniques employed for spiral inertial chips.

3.2.1. Techniques by Deposition

Soft lithography is the most used technique for the fabrication of microfluidic devices, also for the spiral microchannel structure on PDMS substrates. It consists of creating the hard master (often in silicon), pouring liquid polymer (PDMS) into the mold, heat-curing, then subjecting it to a room temperature hardening process; at the end of the procedure, the hardened polymer substrate is peeled off and removed. Soft lithography has the advantage of obtaining high-resolution replicas and three-dimensional geometries with low costs and high production rapidity [61]. Disadvantages of this technique are related to the replica mold and to logistic requirements. First, due to the material softness, in the removing the cast from the mold, pattern deformation may occur [71], then soft lithography requires a cleanroom implying an increase of process costs.

Most spiral microchannel devices reported in literature are fabricated using soft lithography both for rectangular cross-section channels with dimensions ranging from 100 to 500 μm in width and 50 to170 μm in height [34,42,47,50,72–76] and trapezoidal cross-section with dimensions ranging from 200 to 600 μm in width and 40 to 130 μm in height [1,51,52,54,55,77–79]. Trapezoidal cross-section shapes are more challenging to be reproduced than rectangular cross-sections, especially with soft lithography that is limited by the precision achievable with the milling machine in creating the trapezoidal structure on the mold.

The techniques by deposition also include electron-beam lithography, LIGA (lithography-galvanoforming), photolithography, x-ray or laser lithography and xurography [57,58]. Xurography has been used to replicate a rectangular cross-section spiral structure with a variable width from 200 at the inlet to 600 μm at the outlet and a height of 100 μm on a PDMS substrate [80]. The technique involved creating a mold, cutting the design with a plotter, covering it with PDMS and then using a microwave hoven for curing.

These techniques also present some issues: i) they require an additive process for fabricating the patterned mold or the hard master ii) the molds used are usually made of soft materials, causing deformation of the channel geometry when removing the cast from the mold, iii) semi-cleanroom operational conditions are necessary [61]. These aspects increase the costs of such lithography techniques.

3D-printing is an additive manufacturing technique that involves creating three-dimensional structures layer-by-layer according to a CAD model by depositing fused material. Laser selective sintering in a resin bath, powder bed fusion, or inkjet 3D printing are a few examples of additive manufacturing techniques used for the fabrication of micro-devices [57]. The potential of applying 3D-printing to challenging materials as hydrogels has been investigated also by Shen et al.; the group fabricated different microfluidic designs, including a spiral microchannel, based on a hydrosoluble and photo-crosslinkable chitosan methacryloy (CS-MA) [21]. Despite its capability to produce various microfluidic designs with different cross-sections, this technique has limitations in terms of z-resolution during layer-by-layer deposition, especially when structuring hollow channels and voids, which prevents a precise reproduction of the device's geometry. Additionally, some materials (such as polymers, inorganic materials, metals or hydrogels) used in 3D-printing are not transparent, and thus the printed devices are not suitable for real time imaging. Bazaz et al. [78] utilized this technique to prototype a resin (BV-007) spiral microchannel with triangular cross-section of 600 μm in width and 210 μm in height, underlining the flexibility of this method for complex cross-section. Raoufi's group used 3D-printing for prototyping a wax mold of a spiral microchannel with complex cross-section (of a hydraulic diameter of 250 μm) depositing molten wax droplets layer-by-layer; the 3D- printed wax mold was poured with liquid PDMS and curing agent and then let them heat-curing.

3.2.2. Techniques by Removal

 doi:10.20944/preprints202407.1511.v1



Etching involves removing material to create the microfluidic structure via solvent (wet etching) or via plasma or particle beams (dry etching). Although etching enables high processing speeds, wet etching requires the use of corrosive solvents, which poses high safety risks, while dry etching involves long production times and is therefore rarely used. Etching is one of the principal processes for the structuring of materials such as silicon and glass; example of application of this technique for spiral microfluidics is only from [63] on silicon substrates. They used the Bosh process to obtain a spiral channel with cross-sectional dimensions of 100 μm in width and 1250 μm in height. However, they encountered several issues during the etching process due to the thickness of the silicon wafer resulting in difficulties in cooling it; additionally, the etch chemistry caused pocked sidewalls on the features.

Mechanical structuring is based on milling, planing or drilling; they rely on the material structuring using a CNC (Computer Numerical Control) process that transfers the microfluidic structure in CAD (Computer-Aided Design) format to a machine rotating (e.g., milling) or nonrotating cutting tool (e.g., planing) that removes material from the substrate. Mechanical micromilling is still widely used due to its cost-effectiveness, simplicity, process efficiency and rapidity. In spiral microfluidics, it is used for prototyping the microchannel geometry for the mask lithography techniques [8,54]. For example, Ghadami et al., 2017 used micromachining to fabricate a master mold for prototyping a PDMS stair-like microchannel (500 μm in width and 110 μm in height).

Finally, pulsed laser ablation, while requiring expensive equipment, is an effective method for generating multiple microstructures on a variety of materials. This process involves scanning a laser beam over the surface according to the CAD design allowing the removal of material. As the laser beam interacts with the surface, an absorption process occurs, leading to an increase in temperature. Depending on the duration of the laser pulse, thermal degradation induces fusion (for long or short laser pulses) and/or evaporation (for ultrashort pico/femtoseconds laser pulses) of the material. Thanks to the high peak intensities and scanning speeds, pulsed laser ablation allows to obtain the microstructure in a few minutes but could have the disadvantage of deposition of re-solidified material debris around the ablated area, compromising the quality and profile of the microchannels. These drawbacks are eliminated using ultrashort pulses [81–83]. Ultrashort pulsed lasers allow three-dimensional microstructuring on transparent substrates at the wavelength of the laser radiation due to non-linear absorption mechanisms.

For spiral microfluidics, $CO_2$ laser has been used for PMMA surface ablation of trapezoidal cross-section through a grey-scale method [66] and for U/W-shaped cross-section channels [2]. Adel's group used a grey-scale approach in which the intensity and the power of the laser is modulated based on the RBG value of an image. This method allowed for precise control of the laser ablation process to create the trapezoidal cross-section geometry of 600 μm of width, 70 μm of inner height and 110 μm of outer height. Abdel-Mawgood approach consisted of creating the microchannel by a single scan of the defocused laser beam for the U-shaped cross-section, and a double scan for the W-shaped cross-section. Despite the rapidity of this process, they obtained channels without precise dimensions (approximately 220 μm in width and from 162/175 to 210 μm in height) and with a high uncertainty due to short laser pulses.

Instead, a Yb:KGW solid state femtosecond laser was used by Al-Halhouli's group on glass which allowed the structuring of trapezoidal cross-section trapezoidal channels (width of 220 μm, outer height of 60 μm and inner height of 40 μm) with smooth surface channel walls (Al-Halhouli et al., 2018, 2019).

The laser direct writing technique does not need a photomask and a clean room environment, reducing the fabrication time and the cost of the microfluidic chip.

**Table 1.** Material and fabrication techniques for spiral microchannels.

| Material | Fabrication technique | Ref. |
|---|---|---|
| **PMMA** | $CO_2$ laser ablation | [2,66] |

 doi:10.20944/preprints202407.1511.v1



| | | |
|---|---|---|
| **PDMS** | Soft lithography | [1,34,42,47,50–52,54–56,72–77,79,85] |
| | xurography | [80] |
| **Glass** | Yb:KGW solid state laser ablation | [46,84] |
| **Silicon** | etching | [63] |
| **Resin** | 3-D printing | [78] |
| **Hydrogel** | 3D-printing | [68] |
| **Wax** | 3D-printing + soft lihography | [69] |

## 4. Overview on Different Cross-Sectional Shapes

Due to the multiplicity of features of microfluidic structures such as compactness and the high separation efficiency thanks to Dean's secondary flow, scientists have shown interest in developing spiral microfluidic devices. Since the publication of the Di Carlo et al. ([33]) scientific report on particle focusing in curved microchannels, numerous experiments have been conducted to investigate these microfluidic structures.

The main purpose of these studies has been to increase the efficiency of target particle separation, defined as [52,86,87]:

$$SE\ \% = \frac{N_{t,o}}{(N_{t,i})} \cdot 100 \qquad (12)$$

where $N_{t,o}$ is the number of target particles at on outlet, $N_{t,i}$ is total number of particles in the in the channel inlet.

As mentioned in the previous section, the cross-sectional geometry plays a role in the formation of Dean's vortices, enabling the formation of different equilibrium positions and thus facilitating particles sorting. For this reason, scientists have explored the effect of the secondary flow in various cross-sectional shapes over years including rectangular, trapezoidal, triangular, complex/hybrid, cross sections.

In the following pages, an overview of most of the studies of the last two decades about spiral microfluidics is provided. The studies are grouped based on the shape of the channel cross sections, as schematized in Figure 5. An additional section, titled "Combined technique devices", will be dedicated to studies on the combination of inertial focusing in spiral microfluidic devices with different sections and other cell sorting techniques. For each geometry, in each sub-section, information about the type of particles or cells investigated and optimal flow rates to maximize the sorting mechanism and the separation efficiency, are reported.

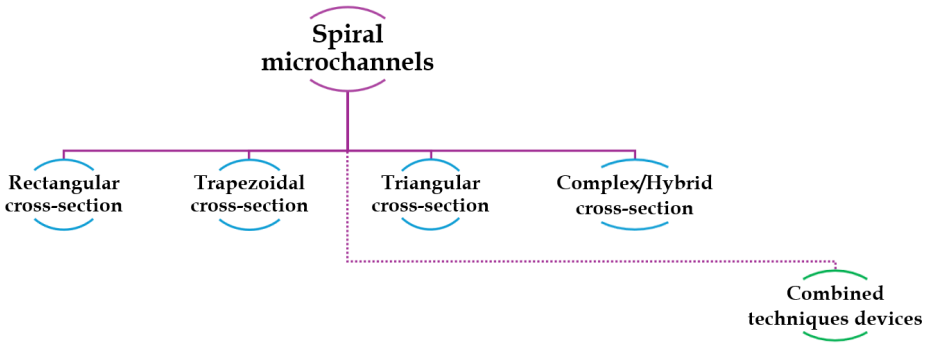


**Figure 5.** Classification spiral microchannels device with different cross-sectional geometries and combined techniques.

The most significant information of each cited study is also summarized in Table 2. which offers to the reader a simplified and complete overview.

### *4.1. Rectangular Cross-Sectional Channels*

 doi:10.20944/preprints202407.1511.v1



The first spiral microfluidic device was proposed in 2007 by Gregoratto's group. The authors designed two devices with spiral geometry on a silicon substrate. The two microfluidic spiral microchannels had a rectangular cross-section with an aspect ratio (AR) of 15 and different channels' lengths, $L_1$=25 cm and $L_2$=50 cm, respectively. For the $L_1$ sample, four symmetric and asymmetric bifurcation with various ratios were chosen, while for the $L_2$ sample, a symmetric bifurcation was employed. The group observed the formation of a single stable Dean vortex after a ¼ loop from the inlet. They noted a significant dependence between the flow rate and the particles concentration collected in each outlet: the highest ratio of particles concentration of inner-outlet to outer-outlet was 3.5 for the $L_2$ device at a flow rate of 2 ml/min. This result was attributed to the device's longer length necessary for particles to reach the focusing equilibrium positions [63].

Subsequently, Bhagat et al. [72] presented a study on a PDMS device with a 5-loop rectangular cross-section spiral microchannel. They first computed numerical simulations of the device behavior, assuming a water solution as liquid medium with polystyrene microparticles of sizes 1.9 and 7.32 μm, respectively, at different flow rates. They found that the device could be used for the separation of fluorescent microbeads at a flow rate of 10 μL/min, achieving a focusing efficiency of 100% of both particles type through the inner and the outer outlet. Consistent with the work of Di Carlo et al. [33], which stated that microbead focusing occurs for $a_p/D_h \geq 0.07$, it was found that particles with diameters below a threshold value of approximately $a_p \approx 5$ μm ($a_p/D_h<0.06$) were more affected by the Dean force than inertial forces, migrating towards the outer channel wall differently from larger particles ($a_p/D_h>0.07$).

In a subsequent study from the same group [42] a device was tested for the separation of larger-sized cells. They designed a 5-loop spiral microchannel with a rectangular cross-section for the separation of fluorescent polystyrene microbeads of 10, 15, and 20 μm diameter (Figure 6a), respectively. By implementing a device with 8 outlets, they successfully separated different microbeads with a separation efficiency of 90% for the three particles sizes at flow rates of approximately 3 μL/min, corresponding to a Dean number of De ~ 14.4. They further tested the device by modifying the cross-section dimensions to W=500 μm and H=120 μm for the separation of SH-SY5Y neuroblastoma cells ($a_p \approx 15$ μm) and C6 glioma cells ($a_p \approx 8$ μm) at a flow rate of 3 μL/min (De ~ 13). They achieved a separation efficiency of ~80% for both the SH-SY5Y cells at outlet 1 and the C6 glioma cells at outlet 2, due to the large variations in the cell sizes (~5 μm) with a 90% cell recovery after 24 hours.

Confirming such promising results obtained by exploiting inertial focusing in spiral microchannels, Nivedita et al. [34] proposed two devices for continuous separation of erythrocytes and leukocytes from a diluted sample of blood. They fabricated two designs of spiral microchannels with rectangular cross section and different aspect ratios: the first device had three-outlet system while the second was designed with a four-outlet system. Testing the devices with polystyrene beads, they observed that in the first device, at the outlet bifurcation, particles all followed the flow and were all collected in the inner outlet, outlet 1, thus no separation was observed. Conversely, in the second device, particles focused in two different flow streams: a broad stream near the inner wall which eluted in the first outlet and a narrow stream, closer to the center of the channel which eluted in the second and third outlet, achieving a high separation efficiency (~95%) at a flow rate of 1-2 mL/min.

Son et al. [88] suggested that a multiple trapezoidal spiral device could enable the mechanical focusing and separation of sperm cells from red blood cells (RBCs) and other debris, such as white blood cells. Sperm cells have irregular shape, but they were assumed to be spherical particles with a diameter of ~5 μm, while RBCs were approximated as spherical particles with a diameter of ~9 μm. At a flow rate of 0.52 mL/min, the device demonstrated the focusing of sperm cells towards the outer wall and RBCs towards the inner wall of the channel. By collecting samples from four different outlets, they achieved a separation efficiency of 81% for non-motile sperm at the outer outlets and 99% for RBCs at the inner outlets.

Warkiani's research group, after two studies on trapezoidal cross section channels [8], published a subsequent study proposing a new rectangular design [47]; they prototyped a 3x multiplexed system consisting of two loops spirals with rectangular section to increase the throughput with

 doi:10.20944/preprints202407.1511.v1



asymmetric outlets. Starting from a flow rate of 100 μm/min, they observed the distribution of the cells across the channel width at the outlet region, using a microscope with a phase-contrast light source and a high-speed camera. They conducted the experiment flowing WBCs and cancer cells separately. The larger particles and cells (>15 μm) did not move in lateral direction once they reached their equilibrium positions near the inner wall. However, while flowing from the inlet, smaller particles and cells moved from the side of the outer wall towards the inner wall, and then back near to the outer wall. They successfully isolated two types of lung and breast CTCs of 12 μm size from BCs, with a flow rate of 1.7 mL/min, despite the presence of some RBCs debris in the output sample, which prevented the precise calculation of the separation efficiency. An innovative spiral structure with rectangular cross section was prototyped by Caffiyar [80] to separate red blood, white blood and dendritic cells from blood fluid. The microchannel had an expanded width from 200 μm at the inlet to 600 μm at the outlet (Figure 6b). This geometry was designed aiming to overcome the defocusing of streamlines and mixing of cells due to the balance between lift and dean forces in narrow channel widths; moreover, they were limited by the low precision of the lithographic technique used in fabricating narrow-width spiral channels. Testing the device both with polystyrene beads and a mixture of human dendritic cells, white blood cells and red blood cells, they reached a separation efficiency of 72% for dendritic cells with an optimal flow rate of 1.5-1.9 mL/min.

Shiriny and Bayareh [86] proposed a single-loop rectangular cross-section channel consisting of two inlets and two outlets to provide a simpler design for industrial fabrication compared to multiple loops (Figure 6c). Mathematical simulations with bloodstream containing WBCs and RBCs along with CTCs (MCF-7 and HeLa) showed approximately 100% separation efficiency at throughput flow rates in the range from 113 to 139 μL/min. From numerical simulations it was expected that MCF-7, HeLa and blood cells had to be focused close to the inner wall of the channel, the central area of the channel, and the area close to the outer channel wall, respectively, thus allowing the three different types of cells to be separated at the three outlets. The separation efficiency of blood cells was 80%, while 100% of MCF-7 and HeLa cells exited from the other two different outlets. Considering separation purity, which is the number of target cells over the total number of cells in one outlet, for MCF-7 cells and blood cells separation purity was 100%, while for HeLa cells was 83% because 20% of blood cells exited from the same outlet.

Magalhães's group demonstrated the possibility of applying inertial focusing to a wide variety of cells [79]. Their study focused on the separation of algal dinoflagellate species of different size from complex seawater samples to increase cell concentration before in situ measurements. Microalgae are mostly between 20 and 60 μm in size (*Alexandrium, Karenia*, and *Dinophysis*) but also a significant portion of species are characterized by smaller cell sizes < 20 μm (*Chlorophyta, Haptophyta, Cyanobacteria*, *Rhodomonas lens* etc.). Using a double rectangular spiral microfluidics, they had to prolong the microchannel length by adding some curves to allow the desegregation of long-chain cell conglomerates (Figure 6d). They also designed an experimental configuration to have recirculation of the solution through a micropumps system for both enhancing *Alexandrium tamarense* concentration through recirculation cycles and selectively collecting *Rhodomonas lens*. Cells separation at the outlets was quantified observing fluorescence emission signal at different wavelengths for both cells. After 3 cycles of circulation with a mixture of *Alexandrium tamarense* (~ 30 μm) and *Rhodomonas lens* (~ 10 μm) at a flow rate of 2000 μL/min, they observed an increase in *Alexandrium tamarense* concentration at outlet 1 reservoir. The recirculation device provided a way to detect samples of low concentrations thanks to selective concentration enrichment before inertial sorting through the microfluidic channel.

The challenge of applying spiral inertial microfluidics to different cells was also demonstrated by Esan et al. [76]. They proposed a rectangular spiral microchannel for separating particles of the same size as bacteria, like e.g., *Escherichia coli* and *Staphylococcus aureus*, from heterogeneous debris extracted from ground meat and meat swabs (Figure 6e). Testing the device with polystyrene beads to mimic the average sizes of bacteria and debris (1.84, 6.04 and 10.6 μm) at 400 μL/min, they observed that 1.84 μm particles ($a_p/D_h$~0.03), which have a size comparable to bacteria, focused near the outer wall of the spiral channel; the 6.04 and 10.6 μm particles ($a_p/D_h$~0.15 and $a_p/D_h$~0.09) focused, instead,

Preprints.org (www.preprints.org) | NOT PEER-REVIEWED | Posted: 19 July 2024 doi:10.20944/preprints202407.1511.v1



near the inner wall of the channel. Using the same device in similar experimental conditions, but flowing the bacterial and ground meats debris suspensions, they determined that the average percentage of debris collected was 49.4% at the inner outlet and 43.4% at the outer outlet, respectively. This result was likely due to the non-homogeneous nature of the debris containing particles smaller than 5 μm.

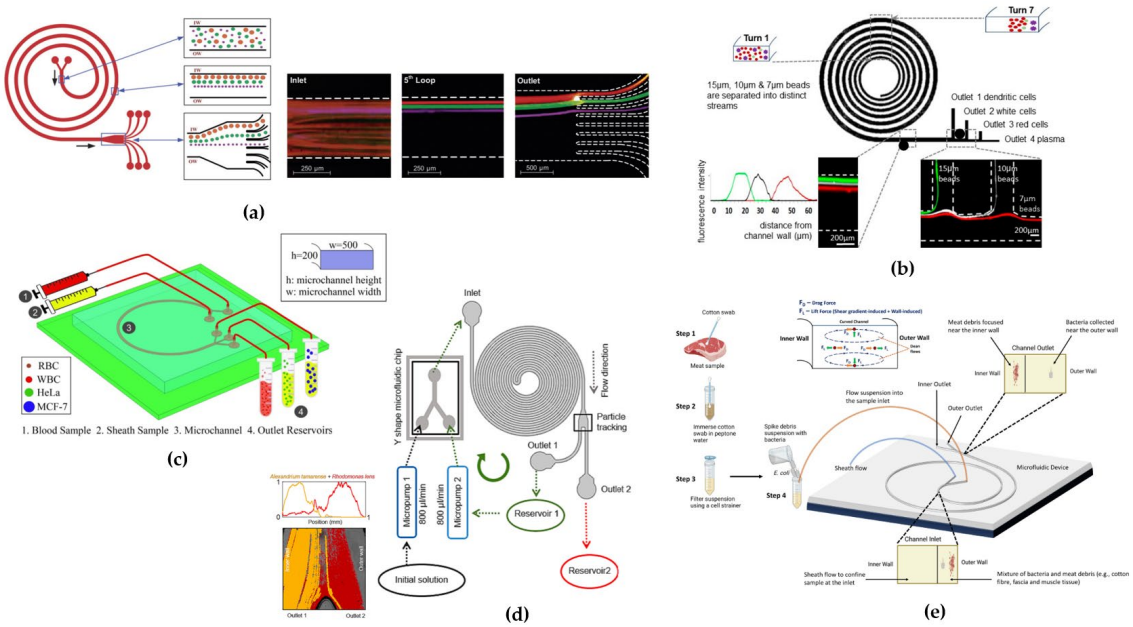


**Figure 6.** (a) Scheme of the spiral microchannel with particles different equilibrium positions along the inner wall (Reprinted with permission from [42]). (b) Spiral microfluidic device with increasing channel widths and images of focused particle of three different sizes streams at the outlets (Reproduced from [80] under http://creativecommons.org/licenses/by/4.0/). (c) Schematic diagram of the microchip device (Reproduced with permission from [86]). (d) Design of the double spiral and tracking representation of *Alexandrium tamarense* and *Rhodomonas lens* at the outlet region (Reproduced from [79] under http://creativecommons.org/licenses/by/4.0/). (g) Illustration of the separation method and microchannel for sorting of Escherichia coli and Staphylococcus aureus (Reproduced from [76] under http://creativecommons.org/licenses/by/4.0/).

### *4.2. Trapezoidal Cross-Sectional Devices*

Many optimizations of channel cross-section and other structural features were made to enhance cells separation through the inertial focusing. By increasing the height of the channel rectangular cross-section, Dean vortices become asymmetric, causing the vortex cores to shift toward the channel depth.

Building on this effect, in [54] it was proposed for the first time a novel spiral channel with trapezoid cross section with two asymmetric outlets (Figure 7a) for separating blood samples containing a high number of haematocrits. This can be problematic due to cell-cell interactions affecting their focusing. The approach that was used relied on increasing the spacing between equilibrium position by fabricating a channel with higher depth towards the outer wall. It was also observed that, in addition to the criterion $a/D_h>0.07$ [33], the height of the inner wall of the channel, was a critical parameter for determining the focus streamlines. Specifically, satisfying the criterion $H_{OUTER}/H_{INNER} > 1.5$ was found to be essential. Polystyrene beads of 6,10, 15.5 μm size were separated at a flow rate of 0.8 mL/min. The device ability in separating polymorphonuclear leukocytes (PMNs) and mononuclear leukocytes (MNLs) from diluted human blood with an efficiency >80% at the same flow rate was also demonstrated. Indeed, under 0.8 mL/min flow rate, PMNs and MNLs formed a focused stream at a distance of ~75 μm away from the inner channel wall, while RBCs migrated to a

 doi:10.20944/preprints202407.1511.v1



broad stream near the outer channel due to smaller cell size. The device was also used as a secondary step of differential centrifugation to further removing RBCs residuals from the isolated WBCs.

Following Wu et al. [54], one of the earliest studies investigating the sorting mechanism of trapezoidal spiral microchannel was conducted by Guan et al. [50]. They compared three 8-loops single-inlet-two-outlet spiral channels, one with a trapezoidal cross section and the other with a rectangular cross section, for particles separation of four different diameters (5.78 μm, 9.77 μm, 15.5 μm, and 26.25 μm) for flow rates in a range from 0.5 to 7.5 mL/min. They noticed that, beyond a threshold flow rate, depending on the radius of the spiral curvature and the slanted angle between the inner and the outer walls, there was an improved separation resolution of particles in the trapezoidal cross-section channel than in the rectangular one. They achieved separation of 15.5 μm from 18.68 μm beads with more than 92% efficiency.

Warkiani's group subsequently proposed two trapezoidal devices. First, they designed an 8-loop microchannel with trapezoidal cross section for the sorting of CTCs (breast adenocarcinoma, bladder and lung cancer cells) from RBCs in a blood sample, achieving an 85% of efficiency with a blood flow rate of 1.7 mL/min [8]. Following this study, they proposed two 8-loop trapezoidal spiral microchannels with different dimensions to demonstrate the application of inertial spiral microfluidic system for the sorting of different types of cells, such as Chinese Hamster Ovary cell and *Saccharomyces cerevisiae* yeast cells (~3–5 μm). For CHO cells, they achieved separation of bigger CHOs (~18 μm) from smaller CHOs (~11 μm) with an efficiency of 92% at a flow rate of 6 mL/min with a single spiral device with cross-section dimensions of 600 μm in width and 80-130 μm in height. For yeast cells, a filtration efficiency of 90% at a flow rate of 2 mL/min was obtained using a trapezoidal microchannel with a width of 450 μm and heights of 30-70 μm. They also designed a multiplexed device combining multiple PDMS layers with spiral microchannels for a continuous size-based separation of large sample volumes (Figure 7b) [51].

Being proved the possibility of applying a label-free spiral devices to separate a variety of cells, a trapezoidal cross-section microchannel was designed by Poon et al. [4] to isolate the osteoprogenitor mesenchymal stromal cells (MSCs) from a heterogeneous culture bone marrow (BM) MSC population. Osteoprogenitor MSCs are interesting as candidates for tissue regenerative therapies, because of the self-renewing stem cells capability [89]. Size-base sorting allows to separate the osteoprogenitor subpopulation (~20 μm) from other MSC subpopulations (~15 μm). A flow rate of 3.0 mL/min was used for size-based cell separation. However, in this work the separation efficiency has not been calculated.

Syed et al. [55] constructed an 8-loop trapezoidal spiral channel to separate and purify *Tetraselmis suecica* (a lipid-rich microalgae) culture from *Phaeodactylum tricornutum* (an invasive diatom). They first tested the device using 6 μm and 10 μm fluorescent polystyrene microbeads to simulate the behavior of microalgae cells. A separation efficiency in range from 90 to 92% was demonstrated for both size of polystyrene microbeads with a flow rate of 1 mL/min. They observed that increasing the flow rate led to a widening of the particles focusing band, causing particles to exit through both outlets due to the action of $F_{Dean}$ force. When utilizing the microalgae solution, they achieved a separation efficiency of 90% for *P. tricornutum* and of 91% for *T. suecica* at a flow rate of 1 mL/min, with a 100% viability of both separated species. They also tested the trapezoidal microchannels to understand the dependence of separation efficiency on concentration, obtaining no significant improvement but, on the contrary, a possible re-contamination of the purified sample.

As in [4], Yin's group [90] identified the "chondrogenic competent" subpopulation of human mesenchymal stem cells (MSCs) through size-dependent serial sorting using a trapezoidal spiral microchannel with asymmetric outlets. The target stem cells in culture had an average size between 17 to 21 μm. The pre-sorted population of MSCs was sequentially pumped through the device for four rounds of sorting. The flow rate was first set at 3.5 mL/min to remove larger cell populations (>21 μm), and then decreased to 1.5 mL/min to remove smaller cell populations (<17 μm). This high-throughput sorting procedure enabled to successfully isolate the medium-sized subpopulation (17-21 μm) from the heterogeneous total population, allowing for the expansion and proliferation of this specific subpopulation.

 doi:10.20944/preprints202407.1511.v1



The study conducted by Al-Halhouli et al. demonstrated the effectiveness of trapezoidal spiral microchannel devices for inertial sorting [46]. They built an 8-loop spiral microchannel fabricated with femtosecond laser ablation on glass (Figure 7c). The device was tested with 5, 10 and 15 μm fluorescent polystyrene microbeads. Through mathematical calculations, they expected that, at flow rates between 1 and 5 mL/min, for the 5 μm particles $F_{Dean}$ was higher than $F_L$, while for the 10 and 15 μm particles $F_L$ was higher than $F_{Dean}$. As confirmed by experimental results, the 5 μm particles focused at the core of the Dean vortices near the outer wall, while the bigger particle focused near the inner wall, achieving high purity of separated particles. The same group [84] tested a second trapezoidal device with 2, 5, 10 μm fluorescent polystyrene microbeads. The experimental results demonstrated good separation of 2 from 5 μm particles at the flow rate of 0.6 mL/min and of 5 from 10 μm particles at the flow rate of 1 mL/min. They also found that below 0.3 mL/min the focusing position was not stable for all particles.

Good results in particle sorting using trapezoidal cross section channel, were also achieved by Condina's researchers' group, who designed a trapezoidal spiral microchannel with asymmetric outlets (Figure 7d) for differentiation of various cell types, including yeasts (*Saccharomyces pastorianus* and *Saccharomyces cerevisiae*) from beer spoilage microorganisms (*Lactobacillus brevis* and *Pediococcus damnosus*). *S. pastorianus* and S. *cerevisiae* have elliptical shape, with average diameters of ~5 μm and ~4 μm, while *L. brevis* and *P. damnosus* have average diameters of ~2.8 μm and ~0.75 μm, respectively. In this study, larger particles (*S. pastorianus*) were focused on the inner wall, while smaller particles (*L. brevis*) were dispersed in the microchannel. To provide additional space for cells to focus, the inner wall was designed to be larger than the outer wall. The device was optimized using cultures in phosphate-buffered saline and lager beer: the focusing efficiency to the inner outlet for *S. pastorianus* was above 90% for 1-2 mL/min flow rates, while for L. *brevis* the efficiency was enhanced from 40% to 90% by separating the sample three times at 1.5 mL/min [1].

Further studies have been conducted to understand how to modify the channel geometry to improve particle focusing and separation. For this reason, Mihandoust et al. [77] proposed two 6-loop microchannels with trapezoidal cross-section, introducing in one of the loops a widening section in the channel outlet (Figure 7e). Testing the device to separate 4, 6 and 10 μm fluorescent microbeads, they observed that the centerline moved towards the inner wall, leading to a disarrangement of the balance between inertial lift and drag forces and pushing smaller particles towards the outer side of the channel. To compare the inertial focusing of both devices, they defined a sharpness factor $s$ ($s = 1 - \frac{b-a}{W}$, $b$ = width of particles focusing bands, $a$ = particle diameter, $W$ = microchannel width). The modified spiral microchannels led to a sorting efficiency of 98% for 6 μm particles at 1.5 mL/min, showing a sharper focusing band.

In [91], inertial focusing in spiral microchannel was employed for auto-perfusion for small-scale culture of suspension cells aiming to replace conventional membrane filters that are subjected to clogging and fouling problems. They demonstrated the performance of the bioreactor system for culturing Chinese hamster ovary (CHO) cells (~ 17.7 μm). The inertial focusing mechanism was first tested with 15.45 μm polystyrene microspheres: with a flow rate of 1.5 mL/min, all the microspheres were sorted to the inner outlet, confirming the focusing at the inner channel wall. The system allowed to achieve cell retention by focusing the cells to the inner outlet, reintroducing them to the cell culture vessel and removing the cell-free waste medium from the outer outlet.

In [66], Adel et al. conducted a study on the fabrication of a trapezoidal spiral microchannel with $CO_2$ laser ablation for the separation of white blood cells (WBCs) from whole blood. For the experimental validation, they tested the device's separation efficiency at different blood dilutions, to reduce the cell-to-cell interaction. They noticed that increasing in the haematocrits concentration (RBCs) lowered the sorting mechanism due to the higher cell-to-cell interaction. With a 1% haematocrits diluted blood sample, they achieved a 90.1% separation efficiency with an optimal flow rate of 800 μL/min and a WBCs recovery rate of 84%.

Preprints.org (www.preprints.org) | NOT PEER-REVIEWED | Posted: 19 July 2024 doi:10.20944/preprints202407.1511.v1



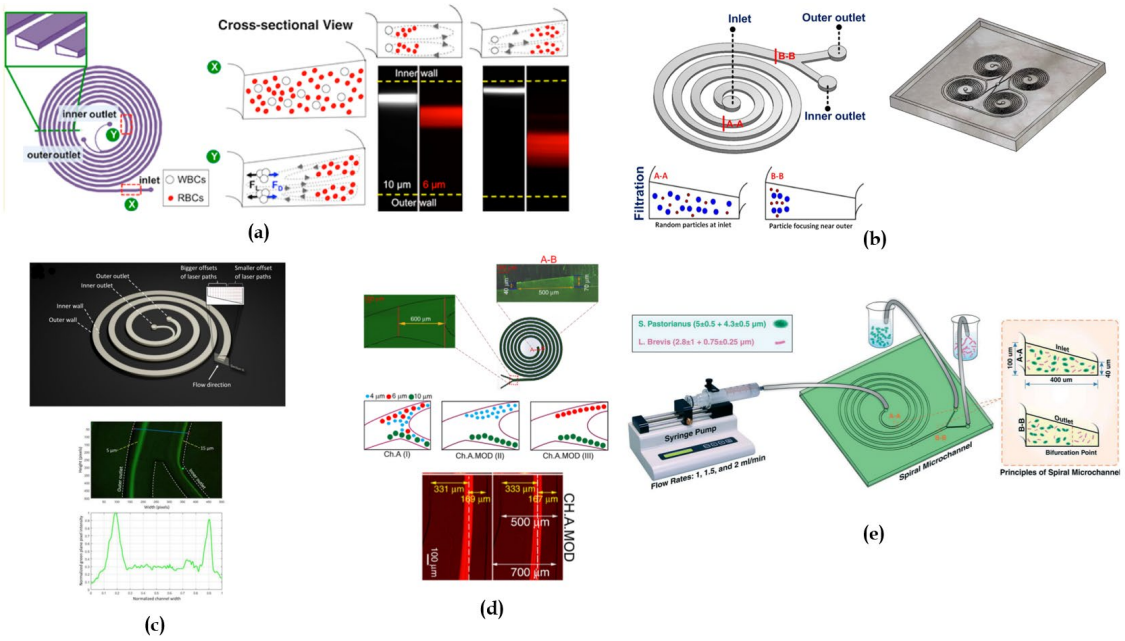


**Figure 7.** (a) Representation of a trapezoidal cross-section spiral microchannel illustrating the principle of particle focusing and trapping within the Dean vortices. Fluorescent images indicating the inertial focusing of 10 µm (white) and 6 µm (red) beads (Reproduced from [54] under http://creativecommons.org/licenses/by/4.0/). (b) 3D drawing of a multiplex device of four spirals connected (Reprinted with permission from [8]) (c) Inverter fluorescent microscope imagine of 5 and 15 µm particles separation in the trapezoidal device (Reproduced from [46] under http://creativecommons.org/licenses/by/4.0/). (d) Schematic illustration of the experimental setup for inertial focusing of S. pastorianus and L. brevis along the inner and outer wall of the channel (Reproduced from [1] under http://creativecommons.org/licenses/by/4.0/). (e) Cross-sectional image of the spiral microchannel with the wider outlet to improve the separation output (Reprinted with permission from [77].

### *4.3. Triangular Cross-Sectional Devices*

Recently, Bazaz et al. [78] fabricated an innovative spiral microchannel with right-angled triangular cross-section and tested it with 5, 7, 10, 13 and 20 µm particles (Figure 8a). Experiments have shown that particles bigger than 10 µm focused in a single tight focusing band at a flow rate of 4 mL/min, while for 20 µm particles a double-band focusing appeared at the same flow rate. This study actually represents the only investigation on the particles focusing behavior in triangular cross-sectional channels.

### *4.4. Hybrid/Hybrid Cross-Sectional Devices*

With the purpose of understanding how by changing the microchannel cross-section the particles equilibrium positions and their focusing is modified, hybrid cross-section shapes, such as a combination of rectangular and trapezoidal geometry, has been investigated. In 2017, Ghadami et al. [56] proposed two geometries: a) rectangular cross section and b) stair like cross section for a 4-loop spiral microchannel. Their study comprised an initial numerical simulation followed by the devices' characterization. Contrary to conventional rectangular spiral microchannels where vortices are positioned latitudinally, the star like design engineered the vortices to be longitudinally placed next to each other. It was found a correlation between the equilibrium position of vortices and the size-dependent flow rate threshold at which vortices stabilized themselves. The stair like geometry allowed increasing the distance between separated particles and thus achieving a high throughput of separation of 7.3 µm from 20 µm particles using a flow rate of ~ 2300 µl/min.

Raoufi's group in 2019 [69], designed a complex cross-sectional channel composed by two trapezoidal sections which led to the formation of two bands, each located in one trapezoidal part,

 doi:10.20944/preprints202407.1511.v1



suggesting that the novel geometry could allow to increase the channel cross-sectional area for high-throughput applications (Figure 8b). They tested the device for separation and purification of Mesenchymal Stem Cells (hMSCs) from microcarriers (dimension of ~ 180 μm) exiting from a perfusion bioreactor, reaching a 98% separation efficiency at a flow rate of 10 mL/min.

Mihandoust's group [52] proposed a novel spiral microchannel with complex cross section consisting of a combination of trapezoidal and rectangular shapes, with the trapezoid section located in the inner region to isolate particles (4 and 6 μm) from the carrier fluid (Figure 8c). The purpose was to design a wider cross-section channel to overcome the limitation of small channel cross-sections that suffer from high fluidic resistance; to achieve cell sorting thanks to inertial forces, microchannels have to adhere to the $a/D_h > 0.07$ criterion restriction which implies too small cross-sectional area. To understand the particle behavior in complex cross-sections, they defined a complex focusing number (CFN) defined by $CFN = \cot\alpha \frac{w_R}{w_T}$ ($\alpha$ = angle between the sloping side and the horizontal line, $w_R$= width of the trapezoid section and $w_T$= width of the rectangular section). The higher the CFN number, the higher the threshold of flow rate required for particles to exit their equilibrium positions. Moreover, after some numerical simulations it was found that the complex cross-section led to narrower focusing bands due to the increase of the fluid velocity in the trapezoidal region. With this design a separation efficiency of approximately 98% was achieved.

As in [52], Saha et al. [92] designed a complex cross-sectional channel with a rectangular and trapezoidal parts to improve isolation efficiency for the sorting of RBCs and WBCs from whole blood. Using computational fluid dynamics (CFD) they confirmed the possibility of enhancing the sorting of these types of cells with a hybrid cross-section.

Another challenging work was recently published by Pan et al. [75]. They designed a rectangular cross section spiral inertial microchannel for studying *Caenorhabditis elegans embryos* at different developmental stages (larvae/adult warms). The channel included side cavities so that particles close to the outer wall of the spiral channel were trapped due to secondary Dean vortices, while particles close to the inner wall bypassed the side cavity (Figure 8d). This design allowed live imaging of single embryos by incorporating features for effective sorting and trapping. Considering the average hydraulic radii of C. elegans embryos and larvae, from ~ 24 to 78 μm, respectively, the channel dimensions were chosen to have $a_p/D_h>0.07$. They achieved separation of embryos from adult worms from a mixture of *C. elegans* with 85% efficiency at a flow rate of 1 mL/min.

A novel cross section geometry was designed also by [2]. The group fabricated two spiral devices with U-shape and W- shaped cross-section geometries to demonstrate the separation of microalgae (*Desmodesmus sp.* ~ 15 μm) from bacterial contaminants (*Escherichia coli* ~ 1 μm) during cultivation (Figure 8e). Experimental tests were conducted in presence or absence of glycine. For the U-device, with glycine, they achieved a separation efficiency of 92% for microalgae and 72% for bacteria, while without glycine they achieved 91% microalgae and 63% bacteria separation efficiencies. For the W-device, with glycine, they achieved a separation efficiency of 96% for microalgae and 87% for bacteria, while 96% microalgae and 66% bacteria separation efficiencies without glycine. Glycine, was used as bacteria chemoattractant, providing extra energy for bacterial migration at target outlet. Additionally, the W-shaped cross-section, thanks to the barrier created at the center of the microchannels during laser ablation, prevented recirculation and mixing of microalgae and bacteria cells improving separation efficiency.

Preprints.org (www.preprints.org) | NOT PEER-REVIEWED | Posted: 19 July 2024 doi:10.20944/preprints202407.1511.v1



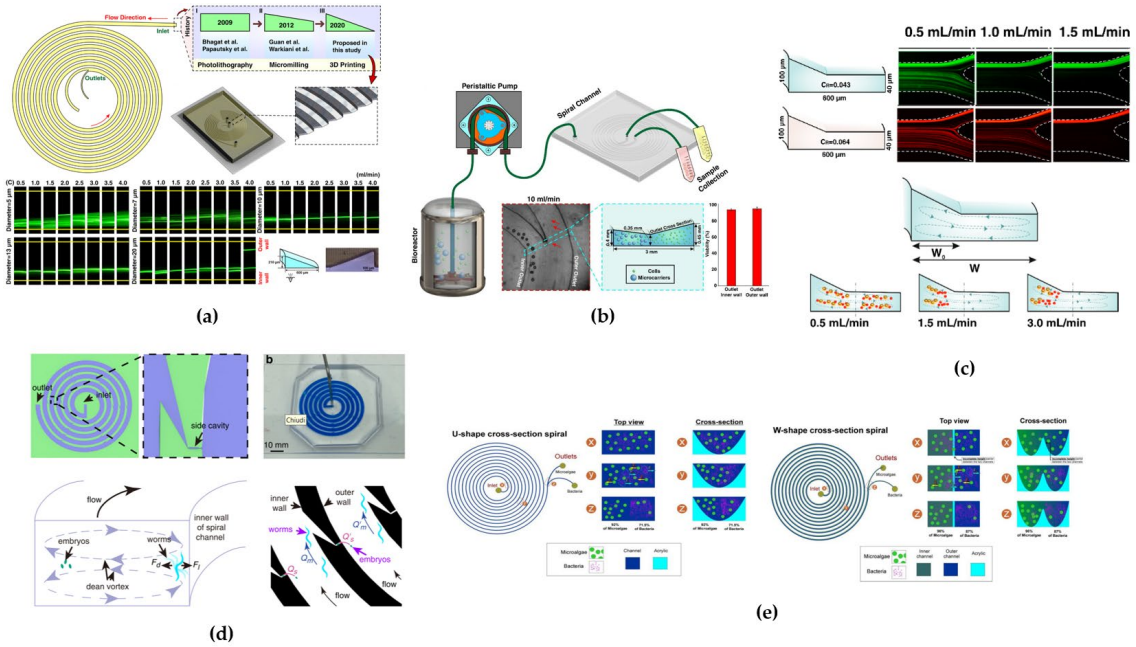


**Figure 8.** (a) Illustration of a right-angled triangular cross-section and images of 10 μm particles focused on a tight band at the outlet of the channel; double-band focusing appears at high flow rates (i.e., 4 ml/min) (Reproduced from [1] under http://creativecommons.org/licenses/by/4.0/). (b) (c) Model of the bioreactor setup for separation of microcarriers from stem cell suspensions. Image of migration of microcarriers to the inner wall before the bifurcation [69]). (c) Schematic of complex cross-section and lateral position for a differential displacement of particles at different flow rates; fluorescent images of the outlet showing the distribution of 4 μm (green) and 6 μm (red) beads at different flow rates (Reproduced from [1]under http://creativecommons.org/licenses/by/4.0/). (d) Microfluidic device for sorting adult worms and embryos in the channel wall cavities (Reproduced from [1] under http://creativecommons.org/licenses/by/4.0/). (e) U-shaped and W-shaped cross-section channel for separation of microalgae and bacteria cells, with microalgae cells occupying the inner outlet and bacteria cells occupying the outer outlet (Reproduced from [2] under http://creativecommons.org/licenses/by/4.0/).

### *4.5. Combined Techniques Devices*

Attempts to increase the spiral microchannels performance have been made by combining inertial sorting technique to other techniques (i.e., passive or active).

In 2017, Kwak's group [6] developed a rectangular spiral microfluidic channel with trapping lateral chambers and a central magnet (Figure 9a). Their aim was to capture two different human breast cancer cell lines (MCF-7 ~ 15-17 μm [93] and MDA-MB-231 ~12 μm [94]) from blood cells through specific conjunction of Epithelial Cell Adhesion Molecule (EpCAM), to magnetic nanoparticles. As previously demonstrated by the same group [95] MCF-7 cells are non-metastatic while MDA-MB-231 cells are metastatic and have positive and negative expression, respectively, so they can be conjugated differently by magnetic nanoparticles. The application of the magnetic field gradient allowed for the selective positioning of heterogenic CTCs. They reached a separation efficiency of 97.2% for MCF-7 cells and 85.1% for MDA-MB-231 cells, respectively, with a flow rate of 150 μL/min.

An interesting study was conducted by Abdulla et al. [73] which aimed to achieve simultaneous separation of two differently sized CTCs (lung cancer cells and breast cancer cells) from blood cells (RBCs and WBCs). They proposed a multiplex cascaded microfluidic chip consisting of two 5-loop spiral channels with different dimension and a zigzag channel (Figure 9b). The Deterministic Lateral Displacement (DLD) was used to combine inertial focusing in spiral channels, which are unable to separate particles or cells with sizes of 20μm and 25μm from each other. Zigzag geometry allowed to use the same flow rate of spiral sections which are not compatible with conventional DLD channels.

Preprints.org (www.preprints.org) | NOT PEER-REVIEWED | Posted: 19 July 2024 doi:10.20944/preprints202407.1511.v1



One of the two spiral channels was connected both with the zigzag part and the other spiral part which respectively ended with two outlets. Testing the device with 5, 8, 15 and 24 μm polystyrene particles to mimic CTCs and BCs: 5 and 8 μm were separated from the spiral channel at a flow rate of 2.2 mL/min, while 15 and 24 μm were separated from the zigzag part at a flow rate of 1.2 mL/min with high efficiency (≤97%). The device was also tested with RBCs-lysed diluted human blood sample performing the separation of WBCs and lung cancer cells from breast cancer cells.

Tabatabaei et al. [85] have tried to enhance the performance of inertial microfluidic devices and increase the purity of the isolated cells by serially integrating a spiral microchannel with a straight microchannel equipped with magnetic actuators. Magnetic separation is an active technique in which the target cells are labelled with magnetic beads by antibodies and then separated applying a magnetic field gradient, while unlabeled cells follow the flow direction. For this reason, this technique can offer more precise control over cells allowing organization of labelled cells [11]. The 4-loop rectangular cross-section spiral microchannel was designed to separate RBCs and WBCs with smaller size from CTCs, followed by a second separation step using magnetic beads for active separation to improve CTCs isolation (Figure 9c). Evaluating the device with 5 μm and 15.3 monodisperse particles, separation efficiencies of 80% and 86%, respectively, at a flow rate of 1200 μL/min were achieved.

Attempts to combine multiple channel geometries were made by Omrani's group [74] which proposed a novel pattern with U-turn combining spiral with trapezoidal cross section and serpentine patterns to increase the focusing of different size cells. Changes in curvature ratio, by introducing a U-turn can influence the Dean flow direction and magnitude, and the maximum velocity location, which depends on the Reynolds number, the curvature ratio, and the cross-section (Figure 9d). In correspondence of the U-turn the maximum velocity moved from the outer wall into the inner wall. As a consequence, when particles pass from the channel segment before to the segment after the U-turn the larger particles migrate from the outer wall to the inner wall while smaller particle move close to the outer wall, increasing the distance between their respective equilibrium positions.

The device was tested with a mixture of monodisperse (5 and 15.6 μm) and polydisperse (2–20 μm) microparticles, obtaining a 94% focusing efficiency at a flow rate of 1.7 mL/min. Then, the spiral microchannel was validated with breast cancer cells to separate BCCs (~ 11-15-18-21 μm) from WBCs (~6-16 μm) (Figure 9d). Introducing the U-shape turn, through numerical simulation, a larger distance between the larger from the smaller particle was observed after the U-shape turn. Experimental test results demonstrated that WBCs and CTCs focusing was possible at flow rate of 1.7 mL/min with about 92% and 93% isolation efficiency, respectively.

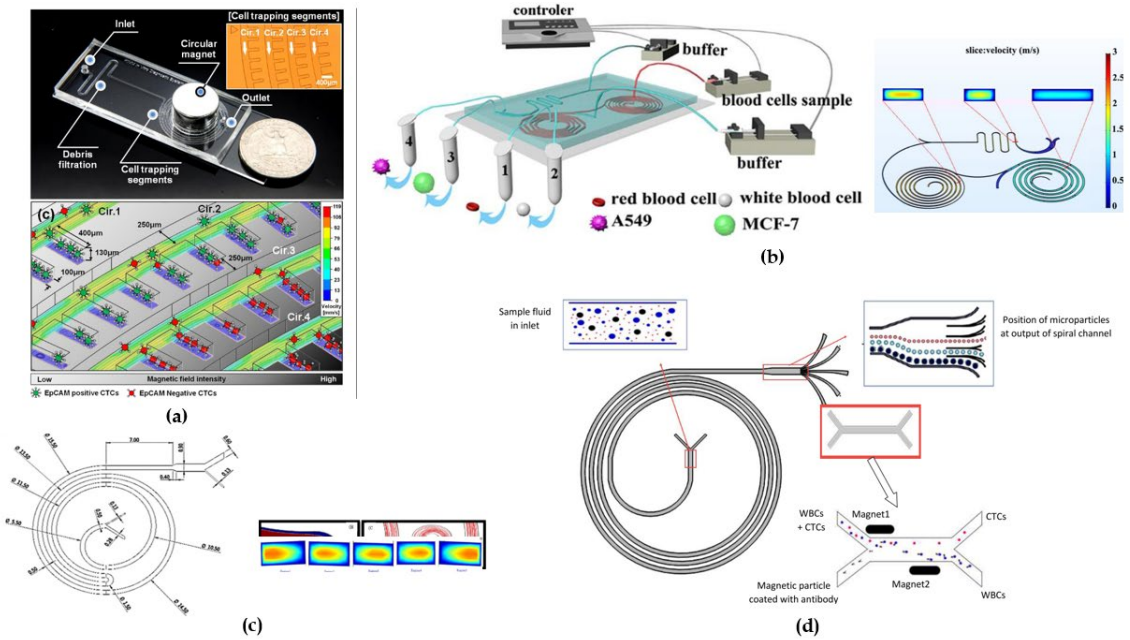

 doi:10.20944/preprints202407.1511.v1



**Figure 9.** (a) Optical image of the spiral shape microfluidic channel with magnetic actuator and microscopic image of two types of breast cancer cells in trapping segments (Reprinted with permission from [6]). (b) Schematic and simulation at optimal flow rate of the cascade spiral and serpentine microfluidic channel (Reprinted with permission from [73]). (c) Illustration of inertial and magnetic spiral sorter for separation of cancer cells from labelled WBCs (Reproduced from [1] under http://creativecommons.org/licenses/by/4.0/). (d) U-turn double spiral microchannel geometric scheme and displacement of maximum velocity after and before of the U-turn (Reproduced from [1] under http://creativecommons.org/licenses/by/4.0/).

**Table 2.** Characteristics of spiral microfluidics studies.

| loop | Channel dimensions | Particles' size | Flowrate | Separation Efficiency (%) | Ref. |
|---|---|---|---|---|---|
| **Rectangular cross section** | | | | | |
| **>10**<br>**>5** | W=100 μm<br>H=1250 μm | polystyrene beads: 1, 8, 10 μm | 2 mL/min | Not specified | [63] |
| **5** | W=100 μm<br>H=50 μm | polystyrene beads=7.32 and 1.9 μm | 10 μL/min | 100% | [72] |
| **5** | W=500 μm<br>H=130 μm | polystyrene beads: 10, 15, 20 μm | 3 mL/min | 90% | [42] |
| | W=500 μm<br>H=120 μm | SH-SY5Y neuroblastoma cells and C6 glioma cells | | 80% | |
| **4** | W=500 μm<br>H=150 μm | RBCs~7 μm<br>WBCs~<br>10-20 μm | 1.8 mL/min | 95% | [34] |
| | W =250 μm<br>H =75 μm | polystyrene beads:<br>7.32, 10, 15 and 20 μm | 1-3 mL/min | All in the first outlets/no separation | |
| **4** | W=150 μm<br>H=50 μm | Sperm cells ~9 μm<br>RBCs ~9 μm | 0.52 μL/min | 81-99% | [88] |
| **3x2** | W=500 μm<br>H=170 μm | polystyrene beads: 6, 10 and 15 μm | 100 μL/min | 90% | [47] |
| | | CTCs>15μm<br>WBCs~7–15 μm | 3 mL/h<br>(0.1mL/min) | | |
| **7** | W=from 200 to 600<br>H=100 | polystyrene beads: 7, 10 and 15 μm<br>Human dendritic cells<br>~ 10-15 μm<br>RBCs~7 μm<br>WBC~7–15 μm | 1.6 mL/min | 72 % | [80] |
| **1** | W=500<br>H=200 | RBCs~7 μm<br>CTCs (HeLa and MCF-7)<br>~ 16-24 μm | ~113-139 mL/h | 100% | [86] |
| **2x5** | W=300 μm<br>H=100μm | polystyrene beads: 6, 10, 20 and 40 μm<br>*algal dinoflagellate* species ~ 20-60 μm | 2000 μL/min | >94%<br>(loss <6%) | [79] |
| **2** | W=200 μm<br>H=70μm | polystyrene beads: 1.84, 6.04 and 10.6 μm<br>bacteria *(Escherichia coli / Staphylococcus aureus)* ~ 1 μm<br>ground meat debris | 400 μL/min | 50% | [76] |
| **Trapezoidal cross section** | | | | | |
| **8** | W=500 μm<br>$H_{in}$=70μm | Polystyrene beads: 6,10, 15.5 μm in water | 0.8 mL/min | >80% | [54] |

 doi:10.20944/preprints202407.1511.v1



| | | | | | |
|---|---|---|---|---|---|
| | $H_{out}$=100µm | polymorphonuclear leukocytes (PMNs), mononuclear leukocytes (MNLs) and haematocrits | | | |
| **8** | W=600 µm<br>$H_{in}$=80µm<br>$H_{ou}$=130µm | Polystyrene beads: 5.8, 9.8, 15.5, 26.25 µm | 0.5-7.5 mL/min | 92% | [50] |
| **8** | W=600 µm<br>$H_{in}$=80µm<br>$H_{ou}$=130µm | RBCs ~ 7 µm<br>different CTCs ~ 15-20 µm | 1700 µL/min | Not specified | [8] |
| **8** | W=600 µm<br>$H_{in}$=80µm<br>$H_{ou}$=130µm | Polystyrene beads: 10 µm and 15 µm<br>Mammalian cells: Chinese Hamster Ovary cells ~ 10-20 µm | 6 mL/min | 92% | [51] |
| | W=450 µm<br>$H_{in}$=30µm<br>$H_{ou}$=70µm | Polystyrene beads: 4 µm<br>Yeast cells: *Saccharomyces cerevisiae* ~ 3-5 µm | 2 mL/min | 90% | |
| **8** | W=600 µm<br>$H_{in}$=80µm<br>$H_{ou}$=130µm | Mesenchymal stem cells (hMSCs) ~ 11-25 µm | 3 mL/min | Not specified | [4] |
| **8** | W=600 µm<br>$H_{in}$=80µm<br>$H_{out}$=130µm | Polystyrene beads: 6 µm and 10 µm<br>Microalgae: *Tetraselmis suecica* ~ 10.7 µm; *Phaeodactylum tricornutum* ~ 25.7 and 3.5 µm | 1 mL/min | 80-91% | [55] |
| **8** | W=580 µm<br>$H_{in}$=85µm<br>$H_{out}$=133µm | Mesenchymal stem cells (hMSCs) ~ 11-25 µm | 1.5 mL/min | Not specified | [90] |
| **8** | W=600 µm<br>$H_{in}$=50µm<br>$H_{out}$=90µm | Polystyrene beads: 5, 10 and 15 µm | 1-5 mL/min | Not specified | [46] |
| **8** | W=200 µm<br>$H_{in}$=40µm<br>$H_{out}$=90µm | Polystyrene beads: 2,5 and 10 µm | 0.6-1 mL/min | Not specified | [84] |
| **4** | W=400 µm<br>$H_{in}$=40µm<br>$H_{out}$=100µm | Beer Spoilage Bacteria ~ 2-5 µm | 1.5 mL/min | 90%/>50% | [1] |
| **6** | W=500 µm<br>$H_{in}$=40µm<br>$H_{out}$=70µm | Polystyrene beads: 4, 6 and 10 µm | 1.5 mL/min | 98% | [77] |
| **6** | W=600 µm<br>$H_{in}$=80µm<br>$H_{out}$=130µm | Polystyrene beads: 15.45 µm<br>Chinese hamster ovary cells ~ 17.7 µm | 1.5 mL/min | Not specified | [91] |
| **8** | W=600 µm<br>$H_{out}$=70µm<br>$H_{in}$=110µm | RBCs ~7 µm<br>WBCs ~ 10-15µm | 800 µL/min | 90% | [66] |
| | | **Triangular cross-section** | | | |
| **5** | W= 600 µm<br>$H_{max}$=210µm<br>$H_{min}$= 0 µm | polystyrene beads: 5, 7, 10, 13 and 20 µm | 4 mL/min | Not specified | [78] |
| | | **Hybrid/complex cross-section** | | | |
| | | **Stair-like** | | | |
| **4** | $W_1$=500 µm<br>$H_1$=110µm<br>$W_2$=100 µm<br>$H_2$=70µm | 7.32 and 20 µm<br>human umbilical vein endothelial cells (HUVEC) and fibroblast cells | 2300 µL/min | Not specified | [56] |
| | | **(rectangular + double trapezoidal)** | | | |

 doi:10.20944/preprints202407.1511.v1



| | | | | | |
|---|---|---|---|---|---|
| **5** | $D_h$ = 250 µm | Microcarriers ~ 180 µm<br>Mesenchymal Stem Cells (hMSCs)~ 15-30 µm | 10 mL/min | 98% | [69] |
| **rectangular + trapezoidal** | | | | | |
| **4.5** | W=400 µm<br>$H_{in}$=40µm<br>$H_{out}$=100µm | Polystyrene beads: 4, 6 and 10 µm | 1.5 mL/min | Not specified | [52] |
| | W=500 µm<br>$H_{in}$=40µm<br>$H_{out}$=100µm | | | Not specified | |
| | W=600 µm<br>$H_{in}$=40µm<br>$H_{out}$=100µm | | | 97-98% | |
| **rectangular + cavities** | | | | | |
| **5** | W=1600 µm<br>H=50µm | *C. elegans embryos* ~ 24 µm<br>*adult worms* ~ 26, 32, 40, 61 and 78 µm | 1 mL/min | 85% | [75] |
| **U-shape and W-shape** | | | | | |
| **10** | W=227 µm<br>$H_{max}$=210µm<br>$H_{min}$=175µm | microalgaes *(Desmodesmus sp)* ~ 15 µm<br>bacteria (*Escherichia coli*) ~ 1 µm | 0.7 mL/min | 92%-72% | [2] |
| | W=220 µm<br>$H_{max}$=210µm<br>$H_{min}$=162µm | | | 96%- 66% | |
| **Combined techniques devices** | | | | | |
| **Rectangular spiral + cavities + magnetic actuator** | | | | | |
| **3.5** | W=250 µm<br>H=130µm | *breast cancer cell lines* (MCF-7 ~ 15-17 µm and MDA-MB-231 ~12 µm)<br>BCs | 150 µL/min | ~ 97 - 85% | [6] |
| **Rectangular spiral + DLD** | | | | | |
| **2 x 5** | W=200 µm<br>H=80µm | Polystyrene beads: 5, 8, 15, and 24µm<br>RBC: 7.34 µm – WBC: ~12µm<br>*lung cancer cells* (A549): ~ 10-15µm<br>*breast cancer cells* (MCF-7): ~15-25µm | 1.2 mL/min – 2.2 mL/min | ≤97% | [73] |
| **Rectangular spiral + magnetic actuator** | | | | | |
| **4** | W=500 µm<br>H=130µm | Monodisperse beads: 5 and 15.6 µm<br>Polydisperse beads: from 2 to 20 µm | 1200 µL/min | 86-80 % | [85] |
| **Rectangular spiral + U turn** | | | | | |
| **4** | W=500 µm<br>H=180µm | polydisperse beads: 10µm; monodispersed beads: 5µm and 15µm | 1.7 mL/min | 93% | [74] |

## 5. Conclusions and Perspectives

This This review presented various studies focused on understanding how different types of cells can be separated in spiral microfluidic channels. It shows that this passive technique can be a highly advantageous option for cell separation and filtration. Although more research is needed to fully understand the physical mechanisms—such as how different-sized and shaped particles move to equilibrium positions depending on the channel's cross-section and the flow speed of the liquid—

 doi:10.20944/preprints202407.1511.v1



this technique appears promising. Spiral devices using inertial sorting can meet the ASSURED criteria proposed by the World Health Organization (WHO). The key points are:

1. Using inexpensive, easy-to-process, recyclable, durable, non-toxic, biocompatible materials suitable for real-time imaging (like PDMS and PMMA) makes these devices potentially Affordable and Delivered.
2. Rapid manufacturing techniques that allow mass production and minimize waste materials make these devices affordable. Although soft lithography is widespread, it has issues such as time-consuming and material-intensive pre-fabrication steps and lower precision achievable for complex shapes. In contrast, additive manufacturing (3D printing) allows for precise fabrication of various geometries, though it is limited by the materials available. Ultra-short laser ablation, while less common, offers high precision, speed, and the ability to work with various materials, including PMMA.
3. Designing these microfluidic structures on few square centimetres, single or multi-layer chips without the need for external mechanical or electrical forces makes them Equipment-free and User-friendly; the capacity to operate under high flow pressure conditions also makes them Robust.
4. By better matching the channel and cross-section dimensions with cell sizes, inertial spiral microchannels could become a Sensitive and Specific sorting technique with high throughput and efficiency.

Despite the advancements achieved with this technology, further studies are needed to improve spiral microchannel devices in terms of the entire system design, including chip fabrication, tubing connections and sample injection, the output and sample collection system, and the identification of the correct geometry based on the type of cells to be analyzed. Improvements in these aspects could extend the use of spiral LoC devices to clinical and automated applications.

**Author Contributions:** Conceptualization, A.V. and R.M.V; methodology, A.V.; investigation, I.P.; data curation, I.P., S.C..; writing—original draft preparation, I.P.; writing—review and editing, all authors; visualization, I.P. A.V.; supervision, A.V. A.A.; funding acquisition, A.A. R.M. All authors have read and agreed to the published version of the manuscript.

**Funding:** This work was supported by MUR in the framework of the PRIN 2022 PNRR Project "Surface and Interface acoustic wave-driven Microfluidic devices BAsed on fs-laser technology for particle sorting (SIMBA)" (grant number: Prot. P2022LMRKB), the project "Quantum Sensing and Modeling for One-Health (QuaSiModO)" (CUP: H97G23000100001) and Project TITAN (PON ARS01_00906).

**Data Availability Statement:** Data will be made available on request.

**Conflicts of Interest:** The authors declare no conflicts of interest.

## References

1. Condina, M.R.; Dilmetz, B.A.; Razavi Bazaz, S.; Meneses, J.; Ebrahimi Warkiani, M.; Hoffmann, P. Rapid Separation and Identification of Beer Spoilage Bacteria by Inertial Microfluidics and MALDI-TOF Mass Spectrometry. *Lab Chip* **2019**, *19*, 1961–1970, doi:10.1039/c9lc00152b.
2. Abdel-Mawgood, A.L.; Ngum, L.F.; Matsushita, Y.; El-Mashtoly, S.F.; Fath El-Bab, A.M.R. Separation of Microalgae from Bacterial Contaminants Using Spiral Microchannel in the Presence of a Chemoattractant. **2024**, doi:10.21203/rs.3.rs-3819436/v1.
3. Xavier, M.; Oreffo, R.O.C.; Morgan, H. Skeletal Stem Cell Isolation: A Review on the State-of-the-Art Microfluidic Label-Free Sorting Techniques. *Biotechnol Adv* 2016, *34*, 908–923.
4. Poon, Z.; Lee, W.C.; Guan, G.; Nyan, L.M.; Lim, C.T.; Han, J.; Van Vliet, K.J. Bone Marrow Regeneration Promoted by Biophysically Sorted Osteoprogenitors From Mesenchymal Stromal Cells. *Stem Cells Transl Med* **2015**, *4*, 56–65, doi:10.5966/sctm.2014-0154.
5. Vaidyanathan, R.; Yeo, T.; Lim, C.T. Microfluidics for Cell Sorting and Single Cell Analysis from Whole Blood. In *Methods in Cell Biology*; Academic Press Inc., 2018; Vol. 147, pp. 151–173 ISBN 9780128142820.
6. Kwak, B.; Lee, J.; Lee, J.; Kim, H.S.; Kang, S.; Lee, Y. Spiral Shape Microfluidic Channel for Selective Isolating of Heterogenic Circulating Tumor Cells. *Biosens Bioelectron* **2018**, *101*, 311–316, doi:10.1016/j.bios.2017.10.036.

7. Mohammadi, A.; Rahmanian, M. Label-Free Isolation of Circulating Tumor Cells Using Lateral Dielectrophoresis- Assisted Inertial. *Microfluid Nanofluidics* **2023**, doi:10.21203/rs.3.rs-2752830/v1.
8. Warkiani, M.E.; Guan, G.; Luan, K.B.; Lee, W.C.; Bhagat, A.A.S.; Kant Chaudhuri, P.; Tan, D.S.W.; Lim, W.T.; Lee, S.C.; Chen, P.C.Y.; et al. Slanted Spiral Microfluidics for the Ultra-Fast, Label-Free Isolation of Circulating Tumor Cells. *Lab Chip* **2014**, *14*, 128–137, doi:10.1039/c3lc50617g.
9. Stephenson, J. *Lab-on-a-Chip Shows Promise in Defining and Diagnosing Cancers*; 1999;
10. Zhang, J.; Yan, S.; Yuan, D.; Alici, G.; Nguyen, N.T.; Ebrahimi Warkiani, M.; Li, W. Fundamentals and Applications of Inertial Microfluidics: A Review. *Lab Chip* 2016, *16*, 10–34.
11. Wyatt Shields Iv, C.; Reyes, C.D.; López, G.P. Microfluidic Cell Sorting: A Review of the Advances in the Separation of Cells from Debulking to Rare Cell Isolation. *Lab Chip* 2015, *15*, 1230–1249.
12. Antoniadi, I.; Skalický, V.; Sun, G.; Ma, W.; Galbraith, D.W.; Novák, O.; Ljung, K. Fluorescence Activated Cell Sorting—A Selective Tool for Plant Cell Isolation and Analysis. *Cytometry Part A* 2022, *101*, 725–736.
13. Yaman, S.; Anil-Inevi, M.; Ozcivici, E.; Tekin, H.C. Magnetic Force-Based Microfluidic Techniques for Cellular and Tissue Bioengineering. *Front Bioeng Biotechnol* 2018, *6*.
14. Bonaccorso, F.; Zerbetto, M.; Ferrari, A.C.; Amendola, V. Sorting Nanoparticles by Centrifugal Fields in Clean Media. *Journal of Physical Chemistry C* **2013**, *117*, 13217–13229, doi:10.1021/jp400599g.
15. Orfao, A.; Ruiz-Arguelles, A. *General Concepts About Cell Sorting Techniques*; 1996; Vol. 29;.
16. Rahman, N.A.; Ibrahim, F.; Yafouz, B. Dielectrophoresis for Biomedical Sciences Applications: A Review. *Sensors (Switzerland)* 2017, *17*.
17. Alnaimat, F.; Dagher, S.; Mathew, B.; Hilal-Alnqbi, A.; Khashan, S. Microfluidics Based Magnetophoresis: A Review. *Chemical Record* 2018, *18*, 1596–1612.
18. Dao, M.; Suresh, S.; Huang, T.J.; Li, P.; Mao, Z.; Peng, Z.; Zhou, L.; Chen, Y.; Huang, P.H.; Truica, C.I.; et al. Acoustic Separation of Circulating Tumor Cells. *Proc Natl Acad Sci U S A* **2015**, *112*, 4970–4975, doi:10.1073/pnas.1504484112.
19. Kim, G.Y.; Han, J.I.; Park, J.K. Inertial Microfluidics-Based Cell Sorting. *Biochip J* 2018, *12*, 257–267.
20. Volpe, A.; Paiè, P.; Ancona, A.; Osellame, R. Polymeric Fully Inertial Lab-on-a-Chip with Enhanced-Throughput Sorting Capabilities. *Microfluid Nanofluidics* **2019**, *23*, doi:10.1007/s10404-019-2206-1.
21. Shen, Y.; Yalikun, Y.; Tanaka, Y. Recent Advances in Microfluidic Cell Sorting Systems. *Sens Actuators B Chem* 2019, *282*, 268–281.
22. Whitesides, G.M. The Origins and the Future of Microfluidics. *Nature* 2006, *442*, 368–373.
23. Mickey Urdea; Laura A. Penny; Stuart S. Olmsted; Maria Y. Giovanni; Peter Kaspar; Andrew Shepherd; Penny Wilson; Carol A. Dahl; Steven Buchsbaum; Gerry Moeller; et al. Requirements for High Impact Diagnostics in Developing World. *Nature* **2006**.
24. De Timàry, G.; Cappello, J.; Scheid, B. Enhanced Pinch Flow Fractionation Using Inertial Streamline Crossing. **2022**, doi:10.21203/rs.3.rs-2026369/v1.
25. McGrath, J.; Jimenez, M.; Bridle, H. Deterministic Lateral Displacement for Particle Separation: A Review. *Lab Chip* 2014, *14*, 4139–4158.
26. Choi, S.; Song, S.; Choi, C.; Park, J.K. Continuous Blood Cell Separation by Hydrophoretic Filtration. *Lab Chip* **2007**, *7*, 1532–1538, doi:10.1039/b705203k.
27. Van Holten, R.W.; Autenrieth, S.; Boose, J.A.; Hsieh, W.-T.; Dolan, S. *Removal of Prion Challenge from an Immune Globulin Preparation by Use of a Size-Exclusion Filter*; 2002;
28. Bhattacharjee, C.; Saxena, V.K.; Dutta, S. Static Turbulence Promoters in Cross-Flow Membrane Filtration: A Review. *Chem Eng Commun* 2020, *207*, 413–433.
29. Paiè, P.; Bragheri, F.; Di Carlo, D.; Osellame, R. Particle Focusing by 3D Inertial Microfluidics. *Microsyst Nanoeng* **2017**, *3*, doi:10.1038/micronano.2017.27.
30. Volpe, A.; Gaudiuso, C.; Ancona, A. Sorting of Particles Using Inertial Focusing and Laminar Vortex Technology: A Review. *Micromachines (Basel)* 2019, *10*.
31. D. J. Tritton *Physical Fluid Dynamics*; 1977; ISBN 978-0-442-30132-3 Published: 01 January 1977.
32. Matas, J.P.; Morris, J.F.; Guazzelli, E. *Lateral Forces on a Sphere Solid/Liquid Dispersions in Drilling and Production Fluides Chargés En Forage et Production Pétrolière*; 2004; Vol. 59;.
33. Di Carlo, D.; Irimia, D.; Tompkins, R.G.; Toner, M. Continuous Inertial Focusing, Ordering, and Separation of Particles in Microchannels. *Proc Natl Acad Sci U S A* **2007**, *104*, 18892–18897, doi:10.1073/pnas.0704958104.
34. Nivedita, N.; Papautsky, I. Continuous Separation of Blood Cells in Spiral Microfluidic Devices. *Biomicrofluidics* **2013**, *7*, doi:10.1063/1.4819275.
35. G. Segrè; A. Silberberg Radial Particle Displacements in Poiseuille Flow. *Nature* **1960**.
36. Smits, A.J. *A Physical Introduction to Fluid Mechanics*; 2024;
37. Tabeling Patrick *Introduction to Microfluidics*; Oxford University Press, Ed.; Second edition.; 2005;
38. Patrick Tabeling *Introduction to Microfluidcs*; 2005;
39. J. Hansson1; J.M. Karlsson2; T. Haraldsson2; W. van der Wijngaart2; A. Russom *INERTIAL PARTICLE FOCUSING IN PARALLEL MICROFLUIDIC CHANNELS FOR HIGH-THROUGHPUT FILTRATION*; IEEE, 2011; ISBN 9781457701566.

40. Asmolov, E.S. *The Inertial Lift on a Spherical Particle in a Plane Poiseuille Flow at Large Channel Reynolds Number*; 1999; Vol. 381;.
41. Zhou, J.; Papautsky, I. Fundamentals of Inertial Focusing in Microchannels. *Lab Chip* **2013**, *13*, 1121–1132, doi:10.1039/c2lc41248a.
42. Kuntaegowdanahalli, S.S.; Bhagat, A.A.S.; Kumar, G.; Papautsky, I. Inertial Microfluidics for Continuous Particle Separation in Spiral Microchannels. *Lab Chip* **2009**, *9*, 2973–2980, doi:10.1039/b908271a.
43. Walz D., G.F. *The Radial Velocity of Spherical Particles in Tubular Pinch Effect Experiments*; 1973;
44. Bhagat, A.A.S.; Kuntaegowdanahalli, S.S.; Papautsky, I. Inertial Microfluidics for Continuous Particle Filtration and Extraction. *Microfluid Nanofluidics* **2009**, *7*, 217–226, doi:10.1007/s10404-008-0377-2.
45. Dean, W.R.; Hurst, J.M.; The London, E. and D.P.M. and J. *XVI Note on the Motion of Fluid in a Curved Pipe*; 1959;
46. Al-Halhouli, A.; Al-Faqheri, W.; Alhamarneh, B.; Hecht, L.; Dietzel, A. Spiral Microchannels with Trapezoidal Cross Section Fabricated by Femtosecond Laser Ablation in Glass for the Inertial Separation of Microparticles. *Micromachines (Basel)* **2018**, *9*, doi:10.3390/mi9040171.
47. Warkiani, M.E.; Khoo, B.L.; Wu, L.; Tay, A.K.P.; Bhagat, A.A.S.; Han, J.; Lim, C.T. Ultra-Fast, Label-Free Isolation of Circulating Tumor Cells from Blood Using Spiral Microfluidics. *Nat Protoc* **2016**, *11*, 134–148, doi:10.1038/NPROT.2016.003.
48. Ramya, S.; Kumar, S.P.; Ram, G.D.; Lingaraja, D. A Short Review of Spiral Microfluidic Devices with Distinct Cross-Sectional Geometries. *Microfluid Nanofluidics* 2022, *26*.
49. Chun, B.; Ladd, A.J.C. Inertial Migration of Neutrally Buoyant Particles in a Square Duct: An Investigation of Multiple Equilibrium Positions. *Physics of Fluids* **2006**, *18*, doi:10.1063/1.2176587.
50. Guan, G.; Wu, L.; Bhagat, A.A.; Li, Z.; Chen, P.C.Y.; Chao, S.; Ong, C.J.; Han, J. Spiral Microchannel with Rectangular and Trapezoidal Cross-Sections for Size Based Particle Separation. *Sci Rep* **2013**, *3*, doi:10.1038/srep01475.
51. Warkiani, M.E.; Tay, A.K.P.; Guan, G.; Han, J. Membrane-Less Microfiltration Using Inertial Microfluidics. *Sci Rep* **2015**, *5*, doi:10.1038/srep11018.
52. Mihandoust, A.; Bazaz, S.R.; Maleki-Jirsaraei, N.; Alizadeh, M.; Taylor, R.A.; Warkiani, M.E. High-Throughput Particle Concentration Using Complex Cross-Section Microchannels. *Micromachines (Basel)* **2020**, *11*, doi:10.3390/MI11040440.
53. Tang, W.; Zhu, S.; Jiang, D.; Zhu, L.; Yang, J.; Xiang, N. Channel Innovations for Inertial Microfluidics. *Lab Chip* 2020, *20*, 3485–3502.
54. Wu, L.; Guan, G.; Hou, H.W.; Bhagat, A.A.S.; Han, J. Separation of Leukocytes from Blood Using Spiral Channel with Trapezoid Cross-Section. *Anal Chem* **2012**, *84*, 9324–9331, doi:10.1021/ac302085y.
55. Syed, M.S.; Rafeie, M.; Vandamme, D.; Asadnia, M.; Henderson, R.; Taylor, R.A.; Warkiani, M.E. Selective Separation of Microalgae Cells Using Inertial Microfluidics. *Bioresour Technol* **2018**, *252*, 91–99, doi:10.1016/j.biortech.2017.12.065.
56. Ghadami, S.; Kowsari-Esfahan, R.; Saidi, M.S.; Firoozbakhsh, K. Spiral Microchannel with Stair-like Cross Section for Size-Based Particle Separation. *Microfluid Nanofluidics* **2017**, *21*, doi:10.1007/s10404-017-1950-3.
57. Waldbaur, A.; Rapp, H.; Länge, K.; Rapp, B.E. Let There Be Chip - Towards Rapid Prototyping of Microfluidic Devices: One-Step Manufacturing Processes. *Analytical Methods* 2011, *3*, 2681–2716.
58. Abgrall, P.; Gué, A.M. Lab-on-Chip Technologies: Making a Microfluidic Network and Coupling It into a Complete Microsystem - A Review. *Journal of Micromechanics and Microengineering* 2007, *17*.
59. Ren, K.; Zhou, J.; Wu, H. Materials for Microfluidic Chip Fabrication. *Acc Chem Res* **2013**, *46*, 2396–2406, doi:10.1021/ar300314s.
60. Roy, E.; Pallandre, A.; Zribi, B.; Horny, M.-C.; Delapierre, F.D.; Cattoni, A.; Gamby, J.; Haghiri-Gosnet, A.-M. Overview of Materials for Microfluidic Applications. In *Advances in Microfluidics - New Applications in Biology, Energy, and Materials Sciences*; InTech, 2016.
61. Gale, B.K.; Jafek, A.R.; Lambert, C.J.; Goenner, B.L.; Moghimifam, H.; Nze, U.C.; Kamarapu, S.K. A Review of Current Methods in Microfluidic Device Fabrication and Future Commercialization Prospects. *Inventions* 2018, *3*.
62. Huang, D.; Man, J.; Jiang, D.; Zhao, J.; Xiang, N. Inertial Microfluidics: Recent Advances. *Electrophoresis* 2020, *41*, 2166–2187.
63. Gregoratto, I.; McNeil, C.J.; Reeks, M.W. Micro-Devices for Rapid Continuous Separation of Suspensions for Use in Micro-Total-Analysis-Systems (MTAS). In Proceedings of the Microfluidics, BioMEMS, and Medical Microsystems V; SPIE, January 20 2007; Vol. 6465, p. 646503.
64. Rodrigues, R.O.; Lima, R.; Gomes, H.T.; Silva, A.M.T. Polymer Microfluidic Devices: An Overview of Fabrication Methods. *U.Porto Journal of Engineering* **2015**, *1*, 67–79, doi:10.24840/2183-6493_001.001_0007.
65. Nielsen, J.B.; Hanson, R.L.; Almughamsi, H.M.; Pang, C.; Fish, T.R.; Woolley, A.T. Microfluidics: Innovations in Materials and Their Fabrication and Functionalization. *Anal Chem* 2020, *92*, 150–168.

66. Adel, M.; Allam, A.; Sayour, A.E.; Ragai, H.F.; Umezu, S.; Fath El-Bab, A.M.R. Fabrication of Spiral Low-Cost Microchannel with Trapezoidal Cross Section for Cell Separation Using a Grayscale Approach. *Micromachines (Basel)* **2023**, *14*, 1340, doi:10.3390/mi14071340.
67. Mohamed, M.G.A.; Ambhorkar, P.; Samanipour, R.; Yang, A.; Ghafoor, A.; Kim, K. Microfluidics-Based Fabrication of Cell-Laden Microgels. *Biomicrofluidics* 2020, *14*.
68. Shen, C.; Li, Y.; She, W.; Meng, Q. Layer-by-Layer Adhesion of Hydrogels for Constructing Heterogeneous Microfluidic Chips. **2023**, doi:10.22541/au.168522147.72071392/v1.
69. Raoufi, M.A.; Razavi Bazaz, S.; Niazmand, H.; Rouhi, O.; Asadnia, M.; Razmjou, A.; Ebrahimi Warkiani, M. Fabrication of Unconventional Inertial Microfluidic Channels Using Wax 3D Printing. *Soft Matter* **2020**, *16*, 2448–2459, doi:10.1039/c9sm02067e.
70. Tumbleston, J.R.; Shirvanyants, D.; Ermoshkin, N.; Janusziewicz, R.; Johnson, A.R.; Kelly, D.; Chen, K.; Pinschmidt, R.; Rolland, J.P.; Ermoshkin, A.; et al. Continuous Liquid Interface Production of 3D Objects. *Science (1979)* **2015**, *347*, 1349–1352, doi:10.1126/science.aaa2397.
71. Bhagat, A.A.S.; Kuntaegowdanahalli, S.S.; Papautsky, I. Continuous Particle Separation in Spiral Microchannels Using Dean Flows and Differential Migration. *Lab Chip* **2008**, *8*, 1906–1914, doi:10.1039/b807107a.
72. Abdulla, A.; Liu, W.; Gholamipour-Shirazi, A.; Sun, J.; Ding, X. High-Throughput Isolation of Circulating Tumor Cells Using Cascaded Inertial Focusing Microfluidic Channel. *Anal Chem* **2018**, *90*, 4397–4405, doi:10.1021/acs.analchem.7b04210.
73. Omrani, V.; Targhi, M.Z.; Rahbarizadeh, F.; Nosrati, R. High-Throughput Isolation of Cancer Cells in Spiral Microchannel by Changing the Direction, Magnitude and Location of the Maximum Velocity. *Sci Rep* **2023**, *13*, doi:10.1038/s41598-023-30275-x.
74. Pan, P.; Qin, Z.; Sun, W.; Zhou, Y.; Wang, S.; Song, P.; Wang, Y.; Ru, C.; Wang, X.; Calarco, J.; et al. A Spiral Microfluidic Device for Rapid Sorting, Trapping, and Long-Term Live Imaging of Caenorhabditis Elegans Embryos. *Microsyst Nanoeng* **2023**, *9*, doi:10.1038/s41378-023-00485-4.
75. Esan, A.; Vanholsbeeck, F.; Swift, S.; McGoverin, C.M. Continuous Separation of Bacterial Cells from Large Debris Using a Spiral Microfluidic Device. *Biomicrofluidics* **2023**, *17*, doi:10.1063/5.0159254.
76. Mihandoust, A.; Maleki-Jirsaraei, N.; Rouhani, S.; Safi, S.; Alizadeh, M. Improvement of Size-Based Particle Separation Throughput in Slanted Spiral Microchannel by Modifying Outlet Geometry. *Electrophoresis* **2020**, *41*, 353–359, doi:10.1002/elps.201900436.
77. Razavi Bazaz, S.; Rouhi, O.; Raoufi, M.A.; Ejeian, F.; Asadnia, M.; Jin, D.; Ebrahimi Warkiani, M. 3D Printing of Inertial Microfluidic Devices. *Sci Rep* **2020**, *10*, doi:10.1038/s41598-020-62569-9.
78. Magalhães, V.; Pinto, V.; Sousa, P.; Gonçalves, L.; Fernández, E.; Minas, G. Spiral Inertial Microfluidics for Separation and Concentration of Phytoplankton. *Algal Res* **2023**, *76*, doi:10.1016/j.algal.2023.103317.
79. Caffiyar, M.Y.; Lim, K.P.; Kamal Basha, I.H.; Hamid, N.H.; Cheong, S.C.; Wei Ho, E.T. Label-Free, High-Throughput Assay of Human Dendritic Cells from Whole-Blood Samples with Microfluidic Inertial Separation Suitable for Resource-Limited Manufacturing. *Micromachines (Basel)* **2020**, *11*, doi:10.3390/mi11050514.
80. Eaton, S.M.; De Marco, C.; Martinez-Vazquez, R.; Ramponi, R.; Turri, S.; Cerullo, G.; Osellame, R. Femtosecond Laser Microstructuring for Polymeric Lab-on-Chips. *J Biophotonics* 2012, *5*, 687–702.
81. Volpe, A.; Trotta, G.; Krishnan, U.; Ancona, A. Prediction Model of the Depth of the Femtosecond Laser Micro-Milling of PMMA. *Opt Laser Technol* **2019**, *120*, doi:10.1016/j.optlastec.2019.105713.
82. Volpe, A.; Krishnan, U.; Chiriacò, M.S.; Primiceri, E.; Ancona, A.; Ferrara, F. A Smart Procedure for the Femtosecond Laser-Based Fabrication of a Polymeric Lab-on-a-Chip for Capturing Tumor Cell. *Engineering* **2021**, *7*, 1434–1440, doi:10.1016/j.eng.2020.10.012.
83. Al-Halhouli, A.; Albagdady, A.; Dietzel, A. Sheath-Less High Throughput Inertial Separation of Small Microparticles in Spiral Microchannels with Trapezoidal Cross-Section. *RSC Adv* **2019**, *9*, 41970–41976, doi:10.1039/c9ra05916d.
84. Tabatabaei, S.A.; Zabetian, M.; Zabetian Targhi, M. Design and Experimental Investigation of a Novel Spiral Microouidic Chip to Separate Wide Size Range of Micro-Particles Design and Experimental Investigation of a Novel Spiral Microfluidic Chip to Separate Wide Size Range of Micro-Particles. **2020**, doi:10.21203/rs.3.rs-64348/v1.
85. Shiriny, A.; Bayareh, M. Inertial Focusing of CTCs in a Novel Spiral Microchannel. *Chem Eng Sci* **2021**, *229*, doi:10.1016/j.ces.2020.116102.
86. McFaul, S.M.; Lin, B.K.; Ma, H. Cell Separation Based on Size and Deformability Using Microfluidic Funnel Ratchets. *Lab Chip* **2012**, *12*, 2369–2376, doi:10.1039/c2lc21045b.
87. Son, J.; Murphy, K.; Samuel, R.; Gale, B.K.; Carrell, D.T.; Hotaling, J.M. Non-Motile Sperm Cell Separation Using a Spiral Channel. *Analytical Methods* **2015**, *7*, 8041–8047, doi:10.1039/c5ay02205c.
88. Keating, A. Mesenchymal Stromal Cells: New Directions. *Cell Stem Cell* 2012, *10*, 709–716.

89. Yin, L.; Wu, Y.; Yang, Z.; Tee, C.A.; Denslin, V.; Lai, Z.; Lim, C.T.; Lee, E.H.; Han, J. Microfluidic Label-Free Selection of Mesenchymal Stem Cell Subpopulation during Culture Expansion Extends the Chondrogenic Potential: In Vitro. *Lab Chip* **2018**, *18*, 878–889, doi:10.1039/c7lc01005b.
90. Yin, L.; Au, W.Y.; Yu, C.C.; Kwon, T.; Lai, Z.; Shang, M.; Warkiani, M.E.; Rosche, R.; Lim, C.T.; Han, J. Miniature Auto-Perfusion Bioreactor System with Spiral Microfluidic Cell Retention Device. *Biotechnol Bioeng* **2021**, *118*, 1951–1961, doi:10.1002/bit.27709.
91. Saha, S.C.; Francis, I.; Nassir, T. Computational Inertial Microfluidics: Optimal Design for Particle Separation. *Fluids* **2022**, *7*, doi:10.3390/fluids7090308.
92. Milo, R.; Jorgensen, P.; Moran, U.; Weber, G.; Springer, M. BioNumbers The Database of Key Numbers in Molecular and Cell Biology. *Nucleic Acids Res* **2009**, *38*, doi:10.1093/nar/gkp889.
93. Truongvo, T.N.; Kennedy, R.M.; Chen, H.; Chen, A.; Berndt, A.; Agarwal, M.; Zhu, L.; Nakshatri, H.; Wallace, J.; Na, S.; et al. Microfluidic Channel for Characterizing Normal and Breast Cancer Cells. *Journal of Micromechanics and Microengineering* **2017**, *27*, doi:10.1088/1361-6439/aa5bbb.
94. Kwak, B.; Lee, J.; Lee, D.; Lee, K.; Kwon, O.; Kang, S.; Kim, Y. Selective Isolation of Magnetic Nanoparticle-Mediated Heterogeneity Subpopulation of Circulating Tumor Cells Using Magnetic Gradient Based Microfluidic System. *Biosens Bioelectron* **2017**, *88*, 153–158, doi:10.1016/j.bios.2016.08.002.
95. Warkiani, M.E.; Guan, G.; Luan, K.B.; Lee, W.C.; Bhagat, A.A.S.; Kant Chaudhuri, P.; Tan, D.S.W.; Lim, W.T.; Lee, S.C.; Chen, P.C.Y.; et al. Slanted Spiral Microfluidics for the Ultra-Fast, Label-Free Isolation of Circulating Tumor Cells. *Lab Chip* **2014**, *14*, 128–137, doi:10.1039/c3lc50617g.